A submerged cylinder wave energy converter with internal sloshing power take off

S.H. Crowley, R. Porter*, D.V. Evans

School of Mathematics, University of Bristol, Bristol, BS8 1TW, UK

Abstract

This paper describes the operation of a new design of wave energy converter. The design consists of a buoyant tethered submerged circular cylinder which is allowed to pitch freely about an axis below its centre. Within the body of the cylinder a fluid half fills an annular tank whose shaped inner walls allow the fundamental sloshing mode of the fluid be to tuned to any period of interest. The pitching motion of the cylinder in waves induces a sloshing motion inside the annular tank which in turns drives an air turbine connecting air chambers above the two isolated internal free surfaces. The concept behind this design is to couple resonances of the pitching cylinder with natural sloshing resonances of the internal water tank and thus achieve a broadbanded power response over a wide range of physically-relevant wave periods. Mathematically, the problem introduces new techniques to solve the series of complex internal forced sloshing problems that arise and to efficiently determine key hydrodynamic coefficients needed for the calculation of the power from the device. The results show that practical configurations can be found in which the efficiency of a two-dimensional cylindrical device is close to its maximum theoretical limit over the target range of periods from 5 to 11 seconds.

Keywords: Wave energy converter, submerged cylinder, coupled resonance, sloshing, broadbanded power.

1. Introduction

Converting the energy of ocean waves into a usable form remains a formidable challenge. This is despite several decades of research and development into different design concepts during which many designs of wave energy converter have been deployed and tested at full-scale. To date there is no clear convergence towards a single design philosophy. Indeed, many of the generic concepts de-

*Corresponding author.

Email addresses: sarah.crowley@bris.ac.uk (S.H. Crowley), richard.porter@bris.ac.uk (R. Porter)

veloped during the early years of wave energy research in the 1970's and early 1980's continue to be reinvented in one form or another.

A successful wave energy converter (WEC) has to be able to address and balance many and varied challenges. Practically, the WEC must be robust enough to survive the harsh marine environment and it must be easy to install and maintain. But the WEC must also be economically viable and fundamentally this requires it to be an efficient converter of wave energy. Balancing these two demands is crucial since no current design is able to boast that it can do both independently better than any other design. Thus, at one end of the scale, theoretical WEC concepts developed to maximise energy capture such as the Salter Duck (Salter [15]) or the Bristol Cylinder (e.g. Clare et al. [5]), have been mainly overlooked because of complex engineering design difficulties. In contrast, many simpler devices have been developed which have low capacity for energy conversion and are thus economically flawed. The Pelamis and Oyster WECs are promising recent examples whose design philosophies set out to balance these two demands. Even so, they have encountered many difficulties which are yet to be fully overcome.

Recently Crowley et al. [3] described a new theoretical concept for a wave energy converter. Although it is based on theoretical ideas of multiple and coupled resonances, previously advocated in Evans and Porter [10], the design also tried to address some of the main practical challenges facing WECs. In particular, the device, being comprised of a cylinder submerged beneath the waves, is protected from the most severe wave forces on the surface of the ocean. In addition, the cylinder's mooring acts as a passive component in the conversion of wave energy – developing a frame of reference against which to take-off power is a key challenge in a converter design. Finally, the confinement of the power take-off mechanism, consisting of a mechanical system of large heavy pendulums connected to dampers, within the body of the cylinder has some desirable practical advantages in terms of maintenance and survivability. Designs based on a similar concept include SEAREV – see Babarit et al. [1]. In constraining the cylinder to move in a predominantly surge motion with respect to incident waves, its two-dimensional theoretical maximum efficiency is limited to 50%; in contrast the Salter Duck or the Bristol Cylinder are theoretically capable of up to 100% maximum efficiency (see, for example, Cruz [6]). In spite of this theoretical compromise made in the design of the device described in Crowley et al. [3], results have suggested that it is capable of operating close to its maximum efficiency over a broad range of (roughly 5-11s) wave periods. Preliminary results for a three-dimensional finite-length cylinder device also suggest capture factors, based on model sea states, of close to one (implying that almost all of the wave energy incident on the length of the cylinder is absorbed). This is significantly higher than the capture factors of roughly 0.55 reported for the nearshore Oyster device and far in excess of the majority of most WECs which typically have a capture factor of below 0.3 – see Babarit et al. [2].

One potential practical disadvantage of the proposed design of Crowley et al. [3] is that the internal pendulums that form the components of the internal

power-take system have to be very big. Thus, in this paper we have considered a different internal power take-off system based on the resonant sloshing motion of a large reservoir of fluid contained within the cylinder. The immediate advantage of this system is that the inertia-effect provided by the heavy pendulums is now replaced by water. Now the incident waves force the cylinder to pitch via its own mooring about an axis below its centre and this then drives the motion of the fluid contained within the internal tank This has shaped inner walls and two isolated internal free surfaces designed so that the internal fluid is resonant at frequencies of interest. In turn, the sloshing motion of the fluid drives air through an electricity-producing Wells-type turbine connecting air chambers above each of the free surfaces. The idea behind the device described above is to couple natural resonances of the pitching cylinder in waves to internal sloshing resonances by selecting particular cylinder geometries, mooring systems and internal tank configurations. The generic idea of coupling wave induced oscillations of floating bodies with internal fluid motions is not new: see, for example, the desalination plant described in Cruz and Salter [7] and in other marine applications in Faltinsen and Timokha [13].

Mathematically, the problem is considered using linearised wave theory and though most of the general wave power theory presented, in Sections 2 and 4, is applicable to devices working in both two-dimensions (practically realised by a cylinder spanning a narrow wave tank) and three-dimensions, results are only presented here for two-dimensional cylinders. The inclusion of an internal water tank increases the complexity of the system considered in Crowley et al. [3] though it is shown in Section 4 that familiar-looking expressions (see, for example, Evans and Porter [10]) for the wave power can be derived. More novel mathematical ideas are developed in Section 5 of the paper which concentrates on the method of solution for certain potentials relating to the forced motion of the internal wave tank which are defined earlier in Section 3. Here, a non-trivial internal tank shape acts as a mechanism for tuning the resonant sloshing frequency and the resulting boundary-value problems are treated analytically using a combination of mathematical techniques. First, the fluid domain is mapped conformally to a composite rectangular domain. Conformal mappings have seen considerable use in analysing sloshing problems in non-trivial domains; see, for example, Fox and Kuttler [14]. The particular geometry chosen allows an eigenfunction expansion matching to be used to develop integral equations for unknown functions relating to the fluid velocity across a line segment in the fluid. This latter part of the solution method is reminiscent of Evans and Fernyhough [12] though the non-trivial mapping of the free surface condition here introduces additional mathematical complexity. It is shown towards the end of Section 5 how each of the hydrodynamic coefficients, representing forces, moments and fluxes, that are needed in the calculation of the power generated by the device are expressed in terms of fundamental properties related to the solution of the integral equations.

The main sets of results are shown in Section 6 and the paper concludes in Section 7.

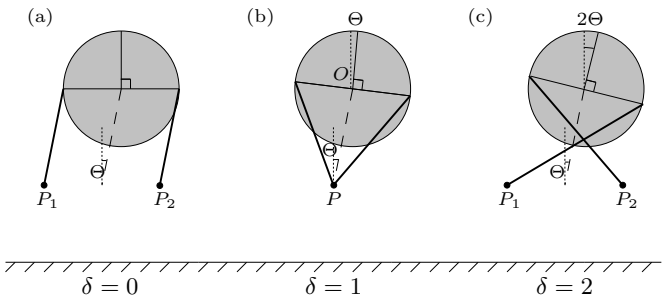

FIGURE 1: Various mooring configurations applied to the submerged horizontal cylinder above the sea bed.

2. Description of the device and its operation

In its most general form, the wave energy converter being considered here is a buoyant cylinder of constant cross section and finite length, which is held submerged below the surface of the fluid by a configuration of tensioned mooring lines which connect it to the sea bed. Figure 1(b) illustrates a cross-section (internal details of the cylinder shown later) through a circular cylinder and the simplest mooring system to be adopted. Thus, the point P represents one of a number (two or more) pivots distributed along the length the cylinder which is assumed to be raised some distance above the bed but held fixed with respect to the bed, perhaps by a number of splayed cables. The tensioned lines which attach P to the cylinder allow the cylinder to pitch about P. Assuming small angles of pitch, $\Theta(t)$, the motion can be decomposed into coupled motions of surge and roll of the cylinder with respect to its local axis, O. Applying simple geometric arguments to figure 1(b) the roll angle is $\Theta(t)$ and the surge displacement is $L\Theta(t)$ where L is the vertical distance OP. The heave displacement is second-order in Θ and neglected.

In a second, more general, version of the mooring system examples of which are shown in figures 1(a),(c), the cylinder is again allowed to pitch via a pair of cables pivoted about two fixed points P_1 and P_2 held fixed at the same level above the sea bed. This system again induces a coupled surge/roll motion of the cylinder about its local axis, O, and, whilst the surge displacement remains $L\Theta(t)$ (where L is now the vertical distance from the midpoint of P_1 and P_2 to O) the pitch-induced roll angle is $\delta\Theta(t)$ where δ is a parameter dictated by the mooring connections of the cables from P_1 and P_2 to the cylinder. If P_1 and P_2 coincide, we return to the first case illustrated in figure 1(b) so that $\delta = 1$. If P_1 and P_2 connect to points on the cylinder directly above P_2 and P_1 (respectively) so that the mooring lines cross each other half way between cylinder and mooring point, then $\delta = 2$, as in figure 1(c). If P_1 and P_2 connect to points on the cylinder directly above P_1 and P_2 (respectively) so that mooring lines are parallel then $\delta = 0$ and there is no pitch-induced roll of the cylinder as in figure 1(a).

Inside the cylinder, an inner cylindrical section of constant cross section runs

along the length of the cylinder and water half fills the annular region between the outer and inner cylindrical sections – see figure 2(a). The operation of this part of the device has already been described in the Introduction. We note that, in practice, the cylinder would be divided along its length into sections and/or contain baffles to mitigate against three-dimensional cross-tank effects.

For reasons of clarity we will initially denote the pitch and roll motions of the cylinder by the variables $\Theta(t)$ and $\Psi(t)$ as though they were independent although these will eventually be coupled as described above via the relation $\Theta = \delta\Psi$.

Cartesian coordinates are used with the origin in the free surface, and z pointing vertically upwards with the central axis of the cylinder, radius b, located along $y = 0$ and $z = -f$. The fluid is of finite depth h.

The forces that act on the cylinder include $F_w(t)$, the wave forces from the external fluid, $F_t(t)$, the forces from the fluid motion in the internal water tank, in addition to hydrostatic restoring forces due to the mooring and buoyancy of the cylinder. Similarly, moments due to waves outside the cylinder are denoted by $D_w(t)$ and due to internal fluid motions by $D_t(t)$. The latter will include, indirectly, the effect of the air turbine in taking energy out of the system.

Assuming small amplitude motions and adopting linearised theory, waves of single frequency ω incident upon the submerged cylinder, induce a response with the same frequency. Writing the forces and moments as $(F_{w,t}(t), D_{w,t}(t)) = \mathrm{Re}\{(X_{w,t}(\omega), T_{w,t}(\omega))\mathrm{e}^{-\mathrm{i}\omega t}\}$ and the surge displacement of O and roll angle about O as $(L\Theta(t), \Psi(t)) = \mathrm{Re}\{(-\mathrm{i}\omega)^{-1}(U(\omega), \Omega(\omega))\mathrm{e}^{-\mathrm{i}\omega t}\}$ the equations of motion are given by

$$-\mathrm{i}\omega MU = X_t + X_w - \frac{\mathrm{i}}{\omega}C_sU, \tag{1}$$

$$-\mathrm{i}\omega I\Omega = T_t + T_w - \frac{\mathrm{i}}{\omega}C_r\Omega, \tag{2}$$

where M is the mass of the cylinder and I its moment of inertia about O. The hydrostatic restoring coefficients C_s and C_r are given by,

$$C_s = (M_w - (M + M_t))\,\frac{g}{L} \qquad \text{and} \qquad C_r = M(z_B - z_G)g. \tag{3}$$

where g is gravitational acceleration, M_w is the mass of water displaced by the cylinder and M_t is the mass of water in the internal tank. Also in (3) $z_B = -f$ is the centre of buoyancy and z_G is the centre of gravity which is computed for the particular configuration considered in Appendix A.

When coupled by the relation $\Omega = \delta U/L$ (1) and (2) can be combined to give

$$-\mathrm{i}\omega M\left(1 + \delta^2(K/L)^2\right)U = \left(X_t + \frac{\delta}{L}T_t\right) + \left(X_w + \frac{\delta}{L}T_w\right) - \frac{\mathrm{i}}{\omega}\left(C_s + \frac{\delta^2}{L^2}C_r\right)U \tag{4}$$

and we have also written $I = MK^2$ in terms of K, the radius of gyration of the cylinder about O.

3. Definition of the hydrodynamic problems

The equations of motion (1), (2) rely upon hydrodynamic forces and moments from both the external and internal fluid motion and these will first be define in terms of the related hydrodynamic problems before coupling (4) to the power-take off element of the device in Section 4.

3.1. The external wave problem

In the exterior of the cylinder we define a velocity potential satisfying

$$\nabla^2\Phi = 0, \qquad \text{in the fluid,} \tag{5}$$

$$\frac{\partial\Phi}{\partial z} + K\Phi = 0, \qquad \text{on } z = 0 \text{ with } K = \omega^2/g, \tag{6}$$

$$\frac{\partial\Phi}{\partial z} = 0, \qquad \text{on } z = -h, \tag{7}$$

where the free surface and the sea bed are located at $z = 0$ and $z = -h$, plus

$$\boldsymbol{n}.\nabla\Phi \equiv \frac{\partial\Phi}{\partial n} = U\boldsymbol{n}.\boldsymbol{i} + \Omega(\boldsymbol{r}\times\boldsymbol{n}).\boldsymbol{j}, \qquad \text{for } \boldsymbol{r}\in S_w \tag{8}$$

where $\boldsymbol{r} = (x, y, z) = x\boldsymbol{i} + y\boldsymbol{j} + (z + f)\boldsymbol{k}$ is measured relative to the axis of rotation O is located along $x = 0$, $z = -f$, and $\boldsymbol{n}$ is the unit normal outward to the fluid to the outer cylinder surface S_w.

Here, we shall be assuming that S_w is a circular cylinder so $(\boldsymbol{r}\times\boldsymbol{n}).\boldsymbol{j} = 0$ for $\boldsymbol{r}\in S_w$ so the final term in (8) vanishes.

Plane waves are obliquely incident from $x = \infty$ and represented by the potential Φ_{inc}. Then $\Phi - \Phi_{inc}$ must represent outgoing waves at infinity.

We decompose Φ into components

$$\Phi = \Phi_d + U\Phi_s \tag{9}$$

where Φ_d, Φ_s represent, respectively, the diffraction of waves by a fixed cylinder and the radiation of waves by a surging cylinder satisfying (5)–(7),

$$\frac{\partial\Phi_d}{\partial n} = 0 \qquad \text{and} \qquad \frac{\partial\Phi_s}{\partial n} = \boldsymbol{n}.\boldsymbol{i}, \qquad \text{for } \boldsymbol{r}\in S_w \tag{10}$$

and $\Phi_d - \Phi_{inc}$ and Φ_s represent outgoing waves at infinity. The total surge wave force X_w on the cylinder is decomposed in line with (9) as $X_w = X_d + UX_s$ where

$$X_{d,s} = -\mathrm{i}\omega\rho\int_{S_w}\Phi_{d,s}\boldsymbol{n}.\boldsymbol{i}\,\mathrm{d}s. \tag{11}$$

It is conventional to decompose the surge-induced wave force due to forced surge motion, X_s, into real and imaginary components as $X_s = \mathrm{i}\omega\mathcal{A}_{ss} - \mathcal{B}_{ss}$ where $\mathcal{A}_{ss}(\omega)$ and $\mathcal{B}_{ss}(\omega)$ are real added mass and radiation damping coefficients for the cylinder in waves.

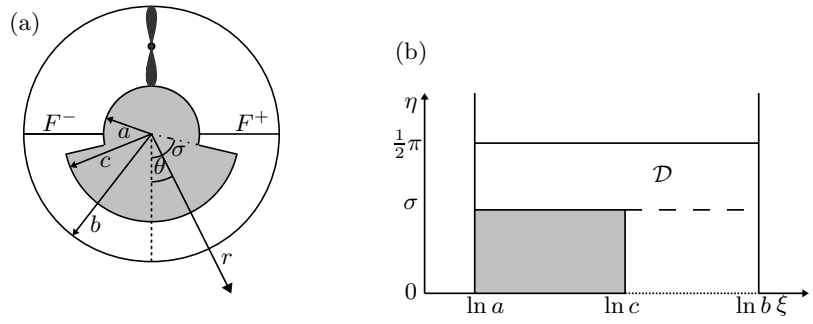

FIGURE 2: (a) Configuration of the internal tank with a wedge-shaped wall protrusion from the inner core; (b) The right-hand side of the fluid domain in transformed coordinates.

In two-dimensions (i.e. an infinitely long cylinder under normal wave incidence) analytic methods based on multipole expansions can be used to compute X_d, $\mathcal{A}_{ss}$ and $\mathcal{B}_{ss}$. For circular cylinders of finite length this has to be done numerically, typically with a panel-based boundary element method such as WAMIT[1].

In summary, the total wave force is written

$$X_w = X_d + U(\mathrm{i}\omega\mathcal{A}_{ss} - \mathcal{B}_{ss}) \tag{12}$$

and $T_w = 0$.

3.2. The internal water tank problem

Re-using Φ for the internal tank problem, we have

$$\nabla^2\Phi = 0, \qquad \text{in the fluid,} \tag{13}$$

$$\frac{\partial\Phi}{\partial z} + K\Phi = \mp\frac{\mathrm{i}\omega}{\rho g}P, \qquad \text{on } z = 0,\ x \in F^{\pm} \tag{14}$$

where $F^{\pm}$ represent the two isolated portions of the free surface to the right and left of the origin and the dynamic air pressures above $F^{\pm}$ are $\mathrm{Re}\{\pm P\mathrm{e}^{-\mathrm{i}\omega t}\}$. On S_t, the inner walls of the cylinder in contact with the fluid,

$$\boldsymbol{n}.\nabla\Phi \equiv \frac{\partial\Phi}{\partial n} = U\boldsymbol{n}.\boldsymbol{i} + \Omega(\boldsymbol{r}\times\boldsymbol{n}).\boldsymbol{j}, \qquad \text{for } \boldsymbol{r}\in S_t. \tag{15}$$

Within the tank, the fluid motion is assumed to be two-dimensional so $\Phi = \Phi(x,z)$. Here we will assume boundaries S_t for which $(\boldsymbol{r}\times\boldsymbol{n}).\boldsymbol{j}$ is not always

[1] www.wamit.com

zero and thus we decompose Φ into three components $\phi^{(s,r,p)}(r,\theta)$ by writing

$$\Phi = U(\phi^{(s)} + r\sin\theta) + \Omega\phi^{(r)} + \frac{\mathrm{i}\omega P}{\rho g}\phi^{(p)}. \tag{16}$$

Polar coordinates are located on O the centre of the cylinder, $x = r\sin\theta$, $z+f = -r\cos\theta$, so that $\boldsymbol{n}.\boldsymbol{i} = r\sin\theta$. The superscripts indicate association with forced surge, roll and free surface pressure motions. Now $\phi^{(s,r,p)}(r,\theta)$ satisfy (13), with

$$\frac{\partial\phi^{(s,r,p)}}{\partial n} = (0, (\boldsymbol{r}\times\boldsymbol{n}).\boldsymbol{j}, 0), \qquad \text{on } \boldsymbol{r}\in S_t \tag{17}$$

and

$$K\phi^{(s,r,p)} - \frac{1}{r}\frac{\partial\phi^{(s,r,p)}}{\partial\theta} = -(Kr, 0, 1), \qquad \text{on } \theta = \tfrac{1}{2}\pi, \text{ or } F^+ \tag{18}$$

with

$$\phi^{(s,r,p)} = 0, \qquad \text{on } \theta = 0. \tag{19}$$

This last equation expresses antisymmetry of the potentials about the centreline of the cylinder; this is on account of the symmetry of S_t about $x = 0$ and the assumed time-harmonicity. Once potentials are determined in $\theta > 0$ they may be extended into $\theta < 0$ using $\phi^{(s,r,p)}(r,\theta) = -\phi^{(s,r,p)}(r,-\theta)$. Note that $\phi^{(s,r,p)}(r,\theta)$ are real potentials, being defined by real boundary-value problems.

Once solutions to the boundary value problems for $\phi^{(s,r,p)}$ are found then we may compute the associated forces and moments from the internal water motion. First, by integrating pressures over the surfaces of the fluid we obtain the force on the cylinder as

$$X_t = \mathrm{i}\omega\rho\int_{S_t}\Phi\,\boldsymbol{n}.\boldsymbol{i}\,\mathrm{d}s \equiv Uf_s + \Omega f_r + Pf_p \tag{20}$$

where

$$f_{s,r,p} = \mathrm{i}\omega\rho\int_{S_t}\left(\phi^{(s)} + r\sin\theta, \phi^{(r)}, \frac{\mathrm{i}\omega}{\rho g}\phi^{(p)}\right)\boldsymbol{n}.\boldsymbol{i}\,\mathrm{d}s. \tag{21}$$

Note that the pressure forces on the free surface do not contribute to the surge force on the cylinder. Note also that f_p is real whilst f_s and f_r are both imaginary. Consequently we write $f_{s,r} = \mathrm{i}\omega A_{ss,rs}$ where A_{ss} and A_{rs} are now real and represent the surge-induced added mass of the internal fluid due to forced surge and roll motion of the cylinder.

Next, the moment on the cylinder due to the internal fluid motion is given by

$$T_t = \mathrm{i}\omega\rho\int_{S_t}\Phi(\boldsymbol{r}\times\boldsymbol{n}).\boldsymbol{j}\,\mathrm{d}s + 2P\int_{F^+}(\boldsymbol{r}\times\boldsymbol{n}).\boldsymbol{j}\,\mathrm{d}s \equiv Ut_s + \Omega t_r + Pt_p \tag{22}$$

where

$$t_{s,r,p} = \mathrm{i}\omega\rho\int_{S_t}\left(\phi^{(s)} + r\sin\theta, \phi^{(r)}, \frac{\mathrm{i}\omega}{\rho g}\phi^{(p)}\right)\boldsymbol{n}.\boldsymbol{i}\,\mathrm{d}s - (0,0,2)\int_{F^+} r\,\mathrm{d}r \tag{23}$$

which now includes the net moment from pressure forces acting on the free surface. Note here that, as before, t_p is real whilst $t_{s,r}$ are imaginary. Thus, we write $t_{s,r} = \mathrm{i}\omega A_{sr,rr}$ where A_{sr} and A_{rr} are real and represent the roll-inertia of the internal fluid due to forced surge and roll motion of the cylinder.

For the purposes of subsequent power calculations, a final hydrodynamic quantity is required from the internal tank problem, namely the integrated flux of air through the turbine which is calculated as the flux of fluid through the portion of the free surface F^+ (which is just minus that across F^- by antisymmetry and conservation of mass) minus the flux due to the cylinder rotation. In other words it is defined by

$$Q = \int_{F^+} \left(\frac{1}{r}\Phi_\theta(r, \tfrac{1}{2}\pi) + \Omega r \right) \mathrm{d}r \equiv U q_s + \Omega q_r + P q_p \tag{24}$$

where

$$q_{(s,r,p)} = \int_{F^+} \left(\frac{1}{r}\phi_\theta^{(s)}, \frac{1}{r}\phi_\theta^{(r)} + r, \frac{\mathrm{i}\omega}{\rho g}\frac{1}{r}\phi_\theta^{(p)} \right) \mathrm{d}r. \tag{25}$$

We note that here q_s and q_r are real whereas q_p is imaginary and, accordingly, write $q_p = \mathrm{i}\omega A_p$ where A_p is now real.

3.3. Reciprocal relations

For readers familiar with hydrodynamic properties of fluid forces in multiple modes of motion, it will come of no surprise that

$$A_{sr} = A_{rs}, \tag{26}$$

an identity established by application of Green's second identity to the potentials $\phi^{(s)}$ and $\phi^{(r)}$. Further applications of Green's identity with other combinations of potentials, namely $\phi^{(p)}$ with $\phi^{(s)}$ and $\phi^{(r)}$ lead to the following key results:

$$f_p = -2q_s, \qquad \text{and} \qquad t_p = -2q_r. \tag{27}$$

For details see Appendix A of Crowley [4].

4. Calculation of power

The mean power generated by the cylinder can be calculated from either

$$W = \mathrm{Re}\{Q\overline{P}\} \qquad \text{or} \qquad W = -\tfrac{1}{2}\mathrm{Re}\{X_t\overline{U} + T_t\overline{\Omega}\} = \tfrac{1}{2}\mathrm{Re}\{X_w\overline{U} + T_w\overline{\Omega}\} \tag{28}$$

where the overbar denotes complex conjugate, noting that the pressure difference across the turbine is $2P$. For the circular cylinder $T_w = 0$ as already discussed and so the right-hand expression simplifies. The equivalence of the two expressions, one measuring the power taken off at the turbine and the other the power generated by the work done moving the cylinder, can be shown through an application of Green's identity to Φ and its complex conjugate inside

the tank. The final step in (28) is made by substituting from the equations of motion (1) and (2). See Appendix A of Crowley [4] for details.

We aim to develop expressions for W in terms of the fundamental hydrodynamic coefficients described in Section 3. Throughout this section, we adopt the coupling $\Omega = (\delta/L)U$ to eliminate Ω in favour of U.

First, from the equation of motion (4) with $T_w = 0$ and (12), we have

$$UZ = \left(X_t + \frac{\delta}{L}T_t\right) + X_d, \tag{29}$$

where,

$$Z = \mathcal{B}_{ss} - \mathrm{i}\omega\left(M\left(1 + \delta^2(K/L)^2\right) + \mathcal{A}_{ss} - \frac{1}{\omega^2}\left(C_s + \frac{\delta^2}{L^2}C_r\right)\right). \tag{30}$$

From (20)–(23) and the discussion that follows each pair of equations, we can write

$$\left(X_t + \frac{\delta}{L}T_t\right) = \mathrm{i}\omega\left(A_{ss} + \frac{\delta}{L}A_{rs} + \frac{\delta}{L}A_{sr} + \frac{\delta^2}{L^2}A_{rr}\right)U + \left(f_p + \frac{\delta}{L}t_p\right)P, \tag{31}$$

where the hydrodynamic coefficients f_p, t_p and A_{ss} etc... are assumed known. Thus we have

$$UZ_1 = X_d + \left(f_p + \frac{\delta}{L}t_p\right)P, \tag{32}$$

where,

$$Z_1 = Z - \mathrm{i}\omega\left(A_{ss} + \frac{2\delta}{L}A_{rs} + \frac{\delta^2}{L^2}A_{rr}\right). \tag{33}$$

after using (26).

We model the effect of the air turbine using a linear relationship between flow rate and pressure difference across the air turbine

$$Q = 2\lambda P, \tag{34}$$

where the turbine parameter, λ, may be real or complex if air compressibility is included (e.g. Sarmento and Falcão [16]).

Using (24), (25) we can write (34) as

$$U\left(q_s + \frac{\delta}{L}q_r\right) = P(2\lambda - \mathrm{i}\omega A_p). \tag{35}$$

and the relation $q_p = \mathrm{i}\omega A_p$, A_p real, has also been used.

Eliminating U between (32) and (35) and rearranging gives

$$\frac{2PZ_1}{\left(q_s + \frac{\delta}{L}q_r\right)}(\lambda + Z_2) = X_d, \tag{36}$$

where,

$$Z_2 = -\tfrac{1}{2}\mathrm{i}\omega A_p + \left(q_s + \frac{\delta}{L}q_r\right)^2 / Z_1, \tag{37}$$

in which we have used the relations (27).

Using the first expression in (28) to calculate the mean power absorbed by the device, we first use (34) to write

$$W = (\lambda + \overline{\lambda})|P|^2, \tag{38}$$

(assuming complex λ for the moment). Substituting in (36) for P gives

$$W = \frac{|X_d|^2}{4}\frac{(\lambda + \overline{\lambda})\left(q_s + \frac{\delta}{L}q_r\right)^2}{|\lambda + Z_2|^2|Z_1|^2}. \tag{39}$$

The identity $2\mathrm{Re}\{Z_2\}(\lambda + \overline{\lambda}) = (|\lambda + Z_2|^2 - |\lambda - \overline{Z}_2|^2)$, can now be used, noting from the definitions of Z_1 and Z_2 in (33) and (37) that

$$|Z_1|^2\mathrm{Re}\{Z_2\} = \left(q_s + \frac{\delta}{L}q_r\right)^2 \mathcal{B}_{ss}, \tag{40}$$

to express the power in the form

$$W = \frac{|X_d|^2}{8\mathcal{B}_{ss}}\left(1 - \frac{|\lambda - \overline{Z}_2|^2}{|\lambda + Z_2|^2}\right). \tag{41}$$

It is evident that

$$W_{max} = |X_d|^2/(8\mathcal{B}_{ss}), \tag{42}$$

coinciding with a well-known result (see, for example, Evans [9]). This maximum power occurs when $\lambda = \overline{Z}_2$ is satisfied, a condition that, in general, requires λ to be complex.

In practice the imaginary part of λ is small and it is often the case theoretically that λ is taken to be real. Then a different route to calculating the power can be taken which results in the expression

$$W = \frac{|X_d|^2}{4}\frac{\left(q_s + \frac{\delta}{L}q_r\right)^2}{|Z_1|^2\left(|Z_2| + \mathrm{Re}\{Z_2\}\right)}\left(1 - \frac{(\lambda - |Z_2|)^2}{|\lambda + Z_2|^2}\right), \tag{43}$$

This reduces further to

$$W = W_{max}\frac{2}{(1 + |Z_2|/\mathrm{Re}\{Z_2\})}\left(1 - \frac{(\lambda - |Z_2|)^2}{|\lambda + Z_2|^2}\right), \tag{44}$$

once (42) and (40) have been used. Now the maximum power attainable for λ real – we call this the optimum power – is given by

$$W_{opt} = \frac{2W_{max}}{(1 + |Z_2|/\mathrm{Re}\{Z_2\})} \tag{45}$$

which is satisfied when $\lambda = |Z_2|$. If $\mathrm{Im}\{Z_2\} = 0$ and $\lambda = \mathrm{Re}\{Z_2\}$, then $W_{opt} = W_{max}$.

In both cases of λ complex and real it has been shown that the calculation of power has been reduced to expressions which depend only on the calculation of the key hydrodynamic coefficients identified in Section 3. The next section outlines how these coefficients are computed.

5. Calculation of the internal tank potentials

5.1. Tank configuration

Figure 2(a) shows the configuration of the internal water tank. The outer surface is circular and of radius b and the inner surface comprises a wedge of angle $2\sigma < \pi$ and radius c protruding symmetrically about the vertical from a circular inner core of radius a. This configuration is chosen to provide the flexibility to tune the natural fundamental sloshing frequency of the internal fluid to values which coincide with periods of interest. This is justified initially by the following arguments. A simple application of Bernoulli's equation applied to a slender U-tube of length L and slowly varying cross section $A(s)$, $0 < s < L$ reveals the natural frequencies to be determined by the relation (see Faltinsen and Timokha [13, §3.6.4])

$$\omega^2 \approx 2g \left(A(0) \int_0^L \frac{\mathrm{d}s}{A(s)} \right)^{-1}. \tag{46}$$

If the U-tube has constant cross section then $\omega^2 \approx 2g/L$ and, maximising L within the cylinder with $L \approx \pi b$, the lowest periods are approximately $\sqrt{2\pi^3 b/g} \approx 2.5\sqrt{b}$. For example, a sloshing period of 10s requires a cylinder radius of the order of 16m; such a size is considered impractical. Instead, (46) shows that the sloshing frequency can be reduced without increasing the size of the cylinder by choosing $A(0)$ to be larger than $A(s)$ along the length of the U-tube. In this way the denominator of (46) is larger than L.

The particular way in which this narrowing of the channel along its length is adopted here, by introducing a step change in the inner wall radius, allows semi-analytic techniques to be used to solve the boundary-value problems of interest for the harmonic potentials $\phi^{(s,r,p)}(r,\theta)$. Thus, in addition to (18) and (19), the boundary condition (17) is now written explicitly for the particular geometry S_t as

$$\phi_r^{(s,r,p)} = 0, \qquad \text{on } S_1, \qquad \text{and} \qquad \frac{1}{r}\phi_\theta^{(s,r,p)} = -(0,r,0), \qquad \text{on } S_2 \tag{47}$$

where S_1 represents the union of the circular inner and outer circular wall sections in $\theta > 0$ and S_2 is the flat face of the wedge along the line $\theta = \sigma$ connecting the two inner circular sections.

5.2. Solution method

In order to solve the three forcing problems in the tank and extract the relevant hydrodynamic coefficients from the solution, we first employ a conformal mapping, $-(z+f)+\mathrm{i}x \equiv r\mathrm{e}^{\mathrm{i}\theta} = \mathrm{e}^{\zeta}$ where $\zeta = \xi + \mathrm{i}\eta$ to the region $0 < \theta < \frac{1}{2}\pi$. Under this transformation, most simply written $r = \mathrm{e}^{\xi}$, $\theta = \eta$, the internal water tank domain is mapped to the composite rectangular domain shown in figure 2(b). Thus S_1 is mapped to vertical line segments aligned with $\xi = \ln a$, $\xi = \ln c$ and $\xi = \ln b$ and S_2 to a horizontal boundary along $\eta = \sigma$. The downward vertical is now the coordinate line $\eta = 0$ and the free surface is mapped to $\eta = \frac{1}{2}\pi$. Under the transformation, $\phi^{(s,r,p)}(r,\theta) = \psi^{(s,r,p)}(\xi,\eta)$ a function satisfying transformed versions of (47), (18) and (19). Specifically, we have

$$\nabla^2\psi^{(\alpha)} = 0, \qquad \text{throughout the fluid,} \tag{48}$$

$$\psi^{(\alpha)} = 0, \qquad \text{on } \eta = 0, \tag{49}$$

$$\psi^{(\alpha)}_{\xi} = 0, \qquad \text{on: } \begin{cases} \xi = \ln a,\ \sigma < \eta < \frac{1}{2}\pi; \\ \xi = \ln c,\ 0 < \eta < \sigma; \\ \xi = \ln b,\ 0 < \eta < \frac{1}{2}\pi, \end{cases} \tag{50}$$

$$\psi^{(\alpha)}_{\eta} = -(0, \mathrm{e}^{2\xi}, 0), \qquad \text{on } \eta = \sigma,\ \ln a < \xi < \ln c, \tag{51}$$

$$K\mathrm{e}^{\xi}\psi^{(\alpha)} - \psi^{(\alpha)}_{\eta} = -(K\mathrm{e}^{2\xi}, 0, \mathrm{e}^{\xi}), \qquad \text{on } \eta = \tfrac{1}{2}\pi,\ \ln a < \xi < \ln b, \tag{52}$$

$\alpha = s, r, p$, relating to the individual surge, roll and pressure problems.

The next step is to exploit the homogeneous wall conditions (50) to write down separation solutions in the two domains above and below the line $\eta = \sigma$, $\ln c < \xi < \ln b$ which we shall denote by Γ. Hence, for $\eta > \sigma$ we can write

$$\psi^{(\alpha)}(\xi,\eta) = \left(a_0^{(\alpha)}\frac{\eta-\sigma}{\frac{1}{2}\pi-\sigma} + b_0^{(\alpha)}\right)\psi_0^I(\xi) + \sum_{n=1}^{\infty}\left(a_n^{(\alpha)}\frac{\sinh p_n(\eta-\sigma)}{\sinh p_n(\frac{1}{2}\pi-\sigma)} + b_n^{(\alpha)}\frac{\cosh p_n(\eta-\sigma)}{\cosh p_n(\frac{1}{2}\pi-\sigma)}\right)\psi_n^I(\xi) \tag{53}$$

and for $\eta < \sigma$ we have

$$\psi^{(\alpha)}(\xi,\eta) = c_0^{(\alpha)}\eta\psi_0^{II}(\xi) + \sum_{n=1}^{\infty} c_n^{(\alpha)}\frac{\sinh q_n\eta}{q_n\cosh q_n\sigma}\psi_n^{II}(\xi). \tag{54}$$

In the above, $\alpha = s, r, p$ and $a_n^{(\alpha)}$, $b_n^{(\alpha)}$ and $c_n^{(\alpha)}$ for $n \geq 0$ are expansion coefficients to be determined. Eigenfunctions in ξ are defined as

$$\psi_n^I(\xi) = \epsilon_n^{-1/2}\cos p_n(\ln b - \xi) \qquad \text{and} \qquad \psi_n^{II}(\xi) = \delta_n^{-1/2}\cos q_n(\ln b - \xi), \tag{55}$$

where

$$p_n = \frac{n\pi}{\ln(b/a)}, \qquad \text{and} \qquad q_n = \frac{n\pi}{\ln(b/c)}. \tag{56}$$

and with

$$\epsilon_n = \tfrac{1}{2}\epsilon_0, \quad \epsilon_0 = \ln(b/a) \qquad \text{and} \qquad \delta_n = \tfrac{1}{2}\delta_0, \quad \delta_0 = \ln(b/c) \tag{57}$$

for $n = 1, 2, \ldots$, such that that two sets of eigenfunctions are orthonormal over their respective intervals:

$$\int_{\ln a}^{\ln b} \psi_n^I(\xi)\psi_m^I(\xi)\,\mathrm{d}\xi = \delta_{mn}, \qquad \text{and} \qquad \int_{\ln c}^{\ln b} \psi_n^{II}(\xi)\psi_m^{II}(\xi)\,\mathrm{d}\xi = \delta_{mn}. \quad (58)$$

The expansions for the potentials expressed in (53) and (54) satisfy (48), (49) and (50). Applying the free surface condition (52) to (53), then multiplying by, first, $\psi_0^I(\xi)$, and then $\psi_m^I(\xi)$ for $m \geq 1$ before integrating over $\ln a < \xi < \ln b$ gives

$$\frac{a_0^{(\alpha)}}{\frac{1}{2}\pi - \sigma} - \sum_{n=1}^{\infty}(a_n^{(\alpha)} + b_n^{(\alpha)})\mathsf{C}_{0n} = d_0^{(\alpha)} + (a_0^{(\alpha)} + b_0^{(\alpha)})\mathsf{C}_{00} \quad (59)$$

and

$$\frac{a_m^{(\alpha)} p_m}{\tanh p_m(\frac{1}{2}\pi - \sigma)} + b_m^{(\alpha)} p_m \tanh p_m(\tfrac{1}{2}\pi - \sigma) - \sum_{n=1}^{\infty}(a_n^{(\alpha)} + b_n^{(\alpha)})\mathsf{C}_{mn} = d_m^{(\alpha)} + (a_0^{(\alpha)} + b_0^{(\alpha)})\mathsf{C}_{m0}, \quad (60)$$

for $m \geq 1$, and $\alpha = s, r, p$ where we have defined

$$\begin{aligned}\mathsf{C}_{mn} &= \int_{\ln a}^{\ln b} K\mathrm{e}^{\xi}\psi_n^I(\xi)\psi_m^I(\xi)\,\mathrm{d}\xi \\ &= \frac{K}{2}(\epsilon_m\epsilon_n)^{-1/2}(b - (-1)^{m+n}a)\left(\frac{1}{1 + (p_n + p_m)^2} + \frac{1}{1 + (p_n - p_m)^2}\right),\end{aligned} \quad (61)$$

for $m, n \geq 0$ and

$$\begin{aligned}d_m^{(s,r,p)} &= \int_{\ln a}^{\ln b} (K\mathrm{e}^{2\xi}, 0, \mathrm{e}^{\xi})\psi_m^I(\xi)\,\mathrm{d}\xi \\ &= \epsilon_m^{-1/2}\left(2K\frac{(b^2 - (-1)^m a^2)}{4 + p_m^2}, 0, \frac{(b - (-1)^m a)}{1 + p_m^2}\right),\end{aligned} \quad (62)$$

for $m \geq 0$. We write (60) in matrix/vector form (practically, this requires truncating the infinite system of algebraic equations at $m, n = N$) as

$$(\mathsf{A} - \mathsf{C})\mathbf{a}^{(\alpha)} + (\mathsf{B} - \mathsf{C})\mathbf{b}^{(\alpha)} = \mathbf{d}^{(\alpha)} + (a_0^{(\alpha)} + b_0^{(\alpha)})\mathbf{C}_0, \quad (63)$$

where the elements of the matrix C and the vector and the $\mathbf{d}^{(\alpha)}$ are defined in (61) and (62) and the vectors $\mathbf{a}^{(\alpha)}$, $\mathbf{b}^{(\alpha)}$ contain the unknown coefficients $a_n^{(\alpha)}$ and $b_n^{(\alpha)}$. Finally, the elements of $\mathbf{C}_0$ are C_{0n} for $n \geq 1$ and A and B are diagonal matrices with entries

$$\mathsf{A}_{mm} = p_m \coth p_m(\tfrac{1}{2}\pi - \sigma), \qquad \text{and} \qquad \mathsf{B}_{mm} = p_m \tanh p_m(\tfrac{1}{2}\pi - \sigma), \quad (64)$$

for $m \geq 1$. Notice at this stage that (59) has not been used. Making $\mathbf{b}^{(\alpha)}$ the subject of (63) gives

$$\mathbf{b}^{(\alpha)} = -\mathbf{a}^{(\alpha)} + \mathsf{P}\mathsf{G}\mathbf{a}^{(\alpha)} + \mathsf{P}\mathbf{d}^{(\alpha)} + (a_0^{(\alpha)} + b_0^{(\alpha)})\mathsf{P}\mathbf{C}_0 \tag{65}$$

where

$$\mathsf{P} = (\mathsf{B} - \mathsf{C})^{-1}, \qquad \text{and} \qquad \mathsf{G} = (\mathsf{B} - \mathsf{A}), \tag{66}$$

such that P is symmetric and G is diagonal with elements

$$\mathsf{G}_{mm} = \frac{-2p_m}{\sinh 2p_m(\frac{1}{2}\pi - \sigma)}. \tag{67}$$

We have to assume that P is invertible in order for it to be evaluated numerically though practically this poses no difficulties.

Finally, we are required to match the potential and its derivatives defined by (53), (54) in the two regions above and below $\eta = \sigma$ along the common interface Γ. In other words, we are to impose the conditions

$$\psi^{(\alpha)}(\xi, \sigma^+) = \psi^{(\alpha)}(\xi, \sigma^-) \qquad \text{and} \qquad \psi_\eta^{(\alpha)}(\xi, \sigma^+) = \psi_\eta^{(\alpha)}(\xi, \sigma^-) \tag{68}$$

for $\ln c < \xi < \ln b$, $\alpha = s, r, p$. We must also apply the condition (51) on the potential in $\eta > \sigma$.

We let $V^{(\alpha)}(\xi)$ denote the unknown value of $\psi_\eta^{(\alpha)}(\xi, \sigma)$ on Γ (i.e. for $\ln c < \xi < \ln b$). It follows from (53) that

$$\int_\Gamma V^{(\alpha)}(\xi)\psi_0^I(\xi)\,\mathrm{d}\xi - e_0^{(\alpha)} = \frac{a_0^{(\alpha)}}{\frac{1}{2}\pi - \sigma}, \tag{69}$$

$$\int_\Gamma V^{(\alpha)}(\xi)\psi_m^I(\xi)\,\mathrm{d}\xi - e_m^{(\alpha)} = \frac{a_m^{(\alpha)} p_m}{\sinh p_m(\frac{1}{2}\pi - \sigma)}, \tag{70}$$

after using (51) and the orthogonality conditions (58) for the set of eigenfunctions in $\eta > \sigma$. Here,

$$e_m^{(\alpha)} \equiv \int_{\ln a}^{\ln c} (0, \mathrm{e}^{2\xi}, 0)\psi_m^I(\xi)\,\mathrm{d}\xi = \left(0, 2\epsilon_m^{-1/2}\frac{(c^2 - (-1)^m a^2)}{4 + p_m^2}, 0\right). \tag{71}$$

Similarly, taking the η-derivative of (54), multiplying the result by $\psi_m^{II}(\xi)$ for $m = 0, 1, 2, \ldots$ and integrating over $(\ln c, \ln b)$ gives

$$\int_\Gamma V^{(\alpha)}(\xi)\psi_m^{II}(\xi)\,\mathrm{d}\xi = c_m^{(\alpha)}, \qquad \text{for } m \geq 0. \tag{72}$$

Next, we apply the first of the conditions (68) to (53) and (54), resulting in

$$\sum_{n=1}^{\infty} \frac{c_n^{(\alpha)}\psi_n^{II}(\xi)}{q_n \coth q_n\sigma} - \sum_{n=1}^{\infty} \frac{b_n^{(\alpha)}\psi_n^I(\xi)}{\cosh p_n(\frac{1}{2}\pi - \sigma)} = b_0^{(\alpha)}\epsilon_0^{-1/2} - c_0^{(\alpha)}\delta_0^{-1/2}\sigma \tag{73}$$

for $\xi \in \Gamma$. Using (65) to eliminate $b_n^{(\alpha)}$ we can rewrite this condition as

$$\sum_{n=1}^{\infty} \frac{a_n^{(\alpha)} \psi_n^I(\xi)}{\cosh p_n(\frac{1}{2}\pi - \sigma)} - \sum_{n=1}^{\infty}\sum_{j=1}^{\infty} \frac{\mathsf{P}_{nj}\mathsf{G}_{jj} a_j^{(\alpha)} \psi_n^I(\xi)}{\cosh p_n(\frac{1}{2}\pi - \sigma)} + \sum_{n=1}^{\infty} \frac{c_n^{(\alpha)} \psi_n^{II}(\xi)}{q_n \coth q_n \sigma}$$
$$= \sum_{n=1}^{\infty}\sum_{j=1}^{\infty} \frac{\mathsf{P}_{nj}\psi_n^I(\xi)}{\cosh p_n(\frac{1}{2}\pi - \sigma)} \left(d_j^{(\alpha)} + (a_0^{(\alpha)} + b_0^{(\alpha)})\mathsf{C}_{j0} \right) + b_0^{(\alpha)} \epsilon_0^{-1/2} - c_0^{(\alpha)} \delta_0^{-1/2} \sigma, \tag{74}$$

for $\xi \in \Gamma$. It follows from substituting for $a_n^{(\alpha)}$ and $c_n^{(\alpha)}$ for $n \geq 1$ from (70) and (72) that

$$\int_{\Gamma} V^{(\alpha)}(t) K(t,\xi)\, \mathrm{d}t = A_1^{(\alpha)} f_1(\xi) + A_2^{(\alpha)} f_2(\xi) + f_\alpha(\xi), \qquad \xi \in \Gamma \tag{75}$$

for $\alpha = s, r, p$. The kernel of the integral operator, $K(t,\xi)$, is real and symmetric and given by,

$$K(t,\xi) = \sum_{n=1}^{\infty}\sum_{j=1}^{\infty} \frac{\mathsf{P}_{nj}\psi_n^I(\xi)\psi_j^I(t)}{\cosh p_n(\frac{1}{2}\pi - \sigma)\cosh p_j(\frac{1}{2}\pi - \sigma)} + \sum_{n=1}^{\infty} \frac{\psi_n^I(\xi)\psi_n^I(t)}{p_n \coth p_n(\frac{1}{2}\pi - \sigma)}$$
$$+ \sum_{n=1}^{\infty} \frac{\psi_n^{II}(\xi)\psi_n^{II}(t)}{q_n \coth q_n \sigma}, \tag{76}$$

where the definition of the matrix elements G_{jj} in (67) have been used. Also in (75)

$$A_1^{(\alpha)} = b_0^{(\alpha)} \epsilon_0^{-1/2} - c_0^{(\alpha)} \delta_0^{-1/2} \sigma, \qquad \text{and} \qquad A_2^{(\alpha)} = a_0^{(\alpha)} + b_0^{(\alpha)}, \tag{77}$$

involve unknown coefficients whilst

$$f_1(\xi) = 1, \qquad f_2(\xi) = \sum_{n=1}^{\infty}\sum_{j=1}^{\infty} \frac{\mathsf{P}_{nj}\mathsf{C}_{j0}\psi_n^I(\xi)}{\cosh p_n(\frac{1}{2}\pi - \sigma)}, \tag{78}$$

and

$$f_\alpha(\xi) = \sum_{n=1}^{\infty}\sum_{j=1}^{\infty} \frac{\mathsf{P}_{nj} d_j^{(\alpha)} \psi_n^I(\xi)}{\cosh p_n(\frac{1}{2}\pi - \sigma)} + \sum_{n=1}^{\infty} \frac{e_n^{(\alpha)} \psi_n^I(\xi)}{p_n \coth p_n(\frac{1}{2}\pi - \sigma)}$$
$$+ \sum_{n=1}^{\infty}\sum_{j=1}^{\infty} \frac{\mathsf{P}_{nj} e_j^{(\alpha)} \psi_n^I(\xi)}{\cosh p_n(\frac{1}{2}\pi - \sigma)\cosh p_j(\frac{1}{2}\pi - \sigma)}, \tag{79}$$

with $\alpha = s, r, p$ are known real functions. Since $d_n^{(\alpha)} = 0$ when $e_n^{(\alpha)} \neq 0$ and vice versa, (79) appears more complicated than it really is.

It follows that if we define five unknowns $V_i(t)$, $i = 1, 2, s, r, p$ as solutions to

$$\int_\Gamma V_i(t)K(t,\xi)\,\mathrm{d}t = f_i(\xi), \qquad \xi \in \Gamma \tag{80}$$

then

$$V^{(\alpha)}(t) = A_1^{(\alpha)}V_1(t) + A_2^{(\alpha)}V_2(t) + V_\alpha(t) \tag{81}$$

will satisfy (75). In principle, $V_i(t)$ are determined as solutions of (80) but the coefficients $A_1^{(\alpha)}$ and $A_2^{(\alpha)}$ remain undetermined and we return to earlier unused equations to determine these.

At this point it is useful to define the 5×5 real matrix T of inner products of $V_i(t)$ with the right-hand side functions $f_j(t)$ defined in (78) and (79). That is,

$$\mathsf{T}_{ij} = \int_\Gamma V_i(t)f_j(t)\,\mathrm{d}t, \qquad \text{for } i,j = 1,2,s,r,p. \tag{82}$$

Using the fact that $K(t,\xi)$ is real and symmetric it can easily be shown that $\mathsf{T}_{ij} = \mathsf{T}_{ji}$.

Using this definition (69) and (72) for $m = 0$ can now be written

$$\left(\frac{a_0^{(\alpha)}}{\frac{1}{2}\pi - \sigma} + e_0^{(\alpha)}\right)\epsilon_0^{1/2} = c_0^{(\alpha)}\delta_0^{1/2} = \int_\Gamma V^{(\alpha)}(\xi)f_1(\xi)\,\mathrm{d}\xi = A_1^{(\alpha)}\mathsf{T}_{11} + A_2^{(\alpha)}\mathsf{T}_{21} + \mathsf{T}_{\alpha 1} \tag{83}$$

for $\alpha = s, r, p$. Recalling the definition of $A_1^{(\alpha)}$ and $A_2^{(\alpha)}$ from (77) we see that the left- and right-hand sides of (83) provide a relation between two unknown coefficients $a_0^{(\alpha)}$ and $b_0^{(\alpha)}$. A second relation is formed from (59) which first requires some attention to deal with the sum over n. Thus, using (65), (70) and subsequently (78) we find that

$$\begin{aligned}\sum_{n=1}^{\infty}(a_n^{(\alpha)} + b_n^{(\alpha)})\mathsf{C}_{0n} = &-\int_\Gamma V^{(\alpha)}(\xi)f_2(\xi)\,\mathrm{d}\xi + \sum_{n=1}^{\infty}\sum_{j=1}^{\infty}\mathsf{P}_{nj}d_j^{(\alpha)}\mathsf{C}_{0n} \\ &+ \sum_{n=1}^{\infty}\sum_{j=1}^{\infty}\frac{\mathsf{P}_{nj}e_j^{(\alpha)}\mathsf{C}_{0n}}{\cosh p_j(\frac{1}{2}\pi - \sigma)} + (a_0^{(\alpha)} + b_0^{(\alpha)})\sum_{n=1}^{\infty}\sum_{j=1}^{\infty}\mathsf{P}_{nj}\mathsf{C}_{j0}\mathsf{C}_{n0}.\end{aligned} \tag{84}$$

This can now be used in (59) to give

$$\frac{a_0^{(\alpha)}}{\frac{1}{2}\pi - \sigma} + A_1^{(\alpha)}\mathsf{T}_{12} + A_2^{(\alpha)}\mathsf{T}_{22} + \mathsf{T}_{\alpha 2} - S_1^{(\alpha)} - A_2^{(\alpha)}S_2 = d_0^{(\alpha)} + A_2^{(\alpha)}\mathsf{C}_{00} \tag{85}$$

for $\alpha = s, r, p$ where

$$S_1^{(s,r,p)} = \sum_{n=1}^{\infty}\sum_{j=1}^{\infty}\mathsf{P}_{nj}\left(d_j^{(s)}, \frac{e_j^{(r)}}{\cosh p_j(\frac{1}{2}\pi - \sigma)}, d_j^{(p)}\right)\mathsf{C}_{0n} \tag{86}$$

and

$$S_2 = \sum_{n=1}^{\infty}\sum_{j=1}^{\infty} \mathsf{P}_{nj}\,\mathsf{C}_{j0}\,\mathsf{C}_{n0}. \tag{87}$$

Now (84) represents the second relation between $a_0^{(\alpha)}$ and $b_0^{(\alpha)}$. In fact it is both easier and sufficient to express these relations in terms of $A_1^{(\alpha)}$ and $A_2^{(\alpha)}$ by noting first that

$$\frac{a_0^{(\alpha)}}{\frac{1}{2}\pi - \sigma} = \gamma_0 \left(A_2^{(\alpha)} - \epsilon_0^{1/2} A_1^{(\alpha)} - \frac{\epsilon_0}{\delta_0}\sigma e_0^{(\alpha)} \right), \quad \text{where } \gamma_0 = 1/(\tfrac{1}{2}\pi - \sigma + \sigma\epsilon_0/\delta_0). \tag{88}$$

Then (83), (85) and (88) may be combined to form the matrix equation for the two unknowns

$$\begin{pmatrix} \mathsf{T}_{11} + \gamma_0\epsilon_0 & \mathsf{T}_{21} - \gamma_0\epsilon_0^{1/2} \\ \mathsf{T}_{12} - \gamma_0\epsilon_0^{1/2} & \mathsf{T}_{22} - S_2 - \mathsf{C}_{00} + \gamma_0 \end{pmatrix} \begin{pmatrix} A_1^{(\alpha)} \\ A_2^{(\alpha)} \end{pmatrix} = \begin{pmatrix} -\mathsf{T}_{\alpha 1} + e_0^{(\alpha)}\gamma_0\epsilon_0^{1/2}(\frac{1}{2}\pi - \sigma) \\ -\mathsf{T}_{\alpha 2} + S_1^{(\alpha)} + d_0^{(\alpha)} + e_0^{(\alpha)}\sigma\gamma_0\epsilon_0/\delta_0 \end{pmatrix}. \tag{89}$$

Let us summarise the method of solution. One must solve the integral equations (80) for each $V_i(\xi)$, use those solutions to calculate the matrix of inner products T_{ij} from (82) and use the results to solve (89) for $A_1^{(\alpha)}$ and $A_2^{(\alpha)}$. As will be shown below this is all that is needed in order to calculate the key properties of the solution. The numerical approximation to the solution of the integral equations is given later.

5.3. Natural sloshing frequencies

We note that the left-hand side 2×2 matrix in (89) is real and symmetric and independent of α. In contrast, each term on the right-hand side of (89) depends on α. If the forcing is turned off in any one mode then (89) reduces to the same homogeneous equation whose non-trivial solutions, determined by the vanishing of the real determinant of the 2×2 matrix, represents the natural sloshing frequencies of the fluid in the tank.

Figures 3(a,b) plot the sloshing frequency parameter $Kb \equiv \omega^2 b/g$ against the channel width ratio $(b-c)/(b-a)$ which varies between 0 (when the wedge cuts off the channel) and 1 (when the the wedge has shrunk to zero leaving a uniform annular tank). The two figures show contrasting ratios of inner core radius to outer tank wall radius, a/b, and within each plot different wedge angles $2\sigma/\pi$ are shown by each of the three curves. It can be seen that increasing a/b towards a narrow U-tube for a uniform annular tank (channel width ratio equal to 1) reduces the fundamental sloshing frequencies to, when $a/b = 0.9$, a value of $Kb \approx 0.66$ close to the value of 0.63 predicted by the slender U-tube formula (46). Values computed for the annular tank have been verified against other methods of solution (see Crowley [4] for details).

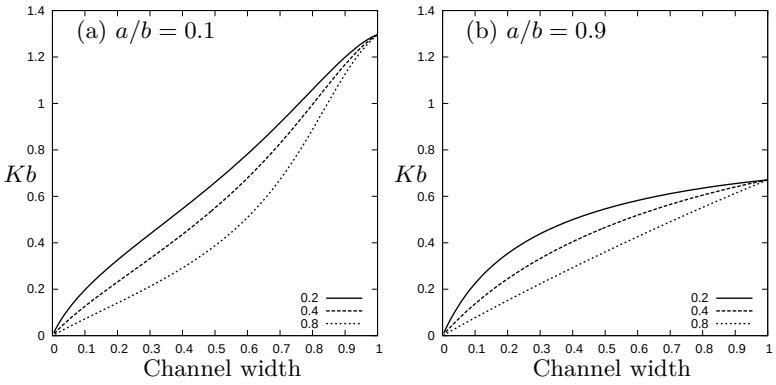

FIGURE 3: The sloshing frequencies of a fluid in a tank of design in Figure 1. In each plot the variation of $Kb \equiv \omega^2 b/g$ is shown against the channel width ratio $(b-c)/(b-a)$, for wedge angles of $2\sigma/\pi = 0.2, 0.4, 0.8$.

We see from figure 3 that increasing the size of the wedge lowers the sloshing frequency parameter Kb. Thus, with b fixed, the sloshing frequency can be made as low as is required. Indeed, this provides us with many different families of tank configuration which can be tuned to any particular frequency. For example, a sloshing frequency of $Kb = 0.2$ can be realised by all six sets of parameters used in figure 3.

5.4. Forces, moments and fluxes

We start with the simplest of the three sets of quantities needed, the free surface fluxes defined by (25). Conservation of mass implies that the integrated flux across the free surface, F^+, is the same as the integrated flux across the line $\eta = \sigma$, $\ln a < \xi < \ln b$ in the transformed plane. In other words, we may write

$$(q_s, q_r, \rho g A_p) = \int_\Gamma \psi_\eta^{(\alpha)}(\xi, \sigma)\, \mathrm{d}\xi + \int_{\ln c}^{\ln b} (0, \mathrm{e}^{2\xi}, 0)\, \mathrm{d}\xi, \tag{90}$$

where $q_p = \mathrm{i}\omega A_p$ and (51) has been used. Using $V^{(\alpha)}(\xi) \equiv \psi_\eta^{(\alpha)}(\xi, \sigma)$ and the decomposition in (81) we have

$$\begin{aligned}(q_s, q_r, \rho g A_p) &= \int_\Gamma V^{(\alpha)}(\xi) f_1(\xi)\, \mathrm{d}\xi + (0, \tfrac{1}{2}(b^2 - c^2), 0) \\ &= A_1^{(\alpha)}\, \mathsf{T}_{11} + A_2^{(\alpha)}\, \mathsf{T}_{21} + \mathsf{T}_{\alpha 1} + (0, \tfrac{1}{2}(b^2 - c^2), 0).\end{aligned} \tag{91}$$

Next, we consider the forces given by (21). The aim is to express the relevant quantities, A_{ss}, A_{rs} and f_p in terms of $A_1^{(\alpha)}$, $A_2^{(\alpha)}$ and the matrix elements T_{ij} as achieved in (91) above. This turns out to be an elongated procedure in which the first step is to note that we can write

$$\boldsymbol{n}.\boldsymbol{i} \equiv \frac{\partial}{\partial n}(r \sin\theta) \equiv \frac{\partial}{\partial n}(\mathrm{e}^\xi \sin\eta) \tag{92}$$

where the normal derivatives apply in the (r,θ)-plane and then the (ξ,η)-plane. Now $\mathrm{e}^{\xi}\sin\eta$ is harmonic and so we may use Green's Identity on the domain $\mathcal{D}$ occupied by the fluid (see figure 2(b)) to write

$$0=\int_{\partial\mathcal{D}}\psi^{(\alpha)}\frac{\partial}{\partial n}(\mathrm{e}^{\xi}\sin\eta)-\mathrm{e}^{\xi}\sin\eta\frac{\partial}{\partial n}\psi^{(\alpha)}\,\mathrm{d}s, \tag{93}$$

where $\partial\mathcal{D}$ is the boundary of $\mathcal{D}$. Then conditions (49)–(52) can be used to write

$$\begin{aligned}0=\int_{\partial\mathcal{D}}\psi^{(\alpha)}\frac{\partial}{\partial n}(\mathrm{e}^{\xi}\sin\eta)\,\mathrm{d}s-\int_{\ln a}^{\ln c}\mathrm{e}^{\xi}\sin\sigma(0,\mathrm{e}^{2\xi},0)\,\mathrm{d}\xi\\ -\int_{\ln a}^{\ln b}\mathrm{e}^{\xi}\left(K\mathrm{e}^{\xi}\psi^{(\alpha)}(\xi,\tfrac{1}{2}\pi)+(K\mathrm{e}^{2\xi},0,\mathrm{e}^{\xi})\right)\,\mathrm{d}\xi.\end{aligned} \tag{94}$$

Also, in transformed coordinates, (21) may be written

$$\left(\frac{A_{ss}}{2\rho},\frac{A_{rs}}{2\rho},\frac{f_p}{-2K}\right)=\int_{\partial\mathcal{D}}\psi^{(\alpha)}\frac{\partial}{\partial n}(\mathrm{e}^{\xi}\sin\eta)\,\mathrm{d}s+(1,0,0)\int_{\partial\mathcal{D}}\mathrm{e}^{\xi}\sin\eta\frac{\partial}{\partial n}(\mathrm{e}^{\xi}\sin\eta)\,\mathrm{d}s, \tag{95}$$

and the second integral evaluates to the half the water area in the tank, that is $M_t/(2\rho)$. Substituting in from (93) and evaluating integrals that arise we find

$$\begin{aligned}\left(\frac{A_{ss}-M_t}{2\rho},\frac{A_{rs}}{2\rho},\frac{f_p}{-2K}\right)=\left(\tfrac{1}{3}K(b^3-a^3),\tfrac{1}{3}(c^3-a^3)\sin\sigma,\tfrac{1}{2}(b^2-a^2)\right)\\ +\int_{\ln a}^{\ln b}K\mathrm{e}^{2\xi}\psi^{(\alpha)}(\xi,\tfrac{1}{2}\pi)\,\mathrm{d}\xi.\end{aligned} \tag{96}$$

In (96) we have been able to express the components of the forces due to surge, roll and pressure in terms of integrals of the potential $\phi^{(\alpha)}$ on the transformed free surface, $\eta=\frac{1}{2}\pi$. However, we would like to be able to express it in terms of the velocities $V^{(\alpha)}\equiv\psi^{(\alpha)}_{\eta}$ across Γ, thereby allowing us to exploit the definitions of the matrix T. To do this we introduce an auxiliary potential, $g(\xi,\eta)$, defined by the artificial problem below, in the upper rectangular region of $\mathcal{D}$ (see figure 2):

$$\nabla^2 g=0, \qquad \text{in } -\ln a<\xi<\ln b,\ \sigma<\eta<\tfrac{1}{2}\pi; \tag{97}$$

$$g_{\eta}=0, \qquad \text{on } \eta=\sigma,\ -\ln a<\xi<\ln b; \tag{98}$$

$$g_{\xi}=0, \qquad \text{on } \xi=\ln a,\ln b,\ \sigma<\eta<\tfrac{1}{2}\pi; \tag{99}$$

$$g_{\eta}-K\mathrm{e}^{\xi}g=K\mathrm{e}^{2\xi}, \qquad \text{on } \eta=\tfrac{1}{2}\pi,\ -\ln a<\xi<\ln b. \tag{100}$$

The solution of this problem is easy to find using separation of variables and gives a general solution

$$g(\xi,\eta)=\beta_0\psi_0^I(\xi)+\sum_{n=1}^{\infty}\beta_n\frac{\cosh p_n(\eta-\sigma)}{\cosh p_n(\tfrac{1}{2}\pi-\sigma)}\psi_n^I(\xi), \tag{101}$$

satisfying (97)–(99). Application of (100) results in the combined infinite systems of equations for the unknown coefficients β_n

$$-\mathbf{C}_0^{\mathrm{T}}\boldsymbol{\beta} = d_0^{(s)} + \beta_0 C_{00}, \tag{102}$$

$$(B - C)\boldsymbol{\beta} = \mathbf{d}^{(s)} + \beta_0 \mathbf{C}_0, \tag{103}$$

where $\boldsymbol{\beta}$ is the vector of coefficients β_n for $n \geq 1$ and C, $\mathbf{d}^{(s)}, d_0^{(s)}$, $\mathbf{C}_0$ and B are all defined previously following (63). It follows that

$$\boldsymbol{\beta} = P(\mathbf{d}^{(s)} + \beta_0 \mathbf{C}_0) \tag{104}$$

where P is defined by (66) and then

$$\beta_0 = -\frac{\mathbf{C}_0^{\mathrm{T}} P \mathbf{d}^{(s)} + d_0^{(s)}}{\mathbf{C}_0^{\mathrm{T}} P \mathbf{C}_0 + C_{00}} \equiv -\frac{S_1^{(s)} + d_0^{(s)}}{S_2 + C_{00}}. \tag{105}$$

The coefficients in (101) are therefore determined in terms of quantities which have already been calculated as part of the solution to the problems described in Section 5.2.

We now apply Green's identity to the potential $\psi^{(\alpha)}$ and $g(\xi, \eta)$ over the rectangle $\sigma < \eta < \frac{1}{2}\pi$, $\ln a < \xi < \ln b$ and employ all the conditions satisfied by these two functions on the boundary of this rectangle to obtain the relation

$$\begin{aligned} 0 = \int_{\ln a}^{\ln b} K\mathrm{e}^{2\xi}\psi^{(\alpha)}(\xi, \tfrac{1}{2}\pi)\,\mathrm{d}\xi - \int_{\ln a}^{\ln b} (K\mathrm{e}^{2\xi}, 0, \mathrm{e}^{\xi}) g(\xi, \tfrac{1}{2}\pi)\,\mathrm{d}\xi \\ + \int_{\Gamma} g(\xi, \sigma) V^{(\alpha)}(\xi)\,\mathrm{d}\xi - \int_{\ln a}^{\ln c} (0, \mathrm{e}^{2\xi}, 0) g(\xi, \sigma)\,\mathrm{d}\xi. \end{aligned} \tag{106}$$

This allows (96) to finally be written

$$\begin{aligned} \left(\frac{A_{ss} - M_t}{2\rho}, \frac{A_{rs}}{2\rho}, \frac{f_p}{-2K}\right) = \sum_{n=0}^{\infty} \beta_n \left(d_n^{(s)}, \frac{e_n^{(r)}}{\cosh p_n(\frac{1}{2}\pi - \sigma)}, d_n^{(p)}\right) \\ - \beta_0 \epsilon_0^{-1/2} \int_{\Gamma} V^{(\alpha)}(\xi) f_1(\xi)\,\mathrm{d}\xi - \beta_0 \int_{\Gamma} V^{(\alpha)}(\xi) f_2(\xi)\,\mathrm{d}\xi - \int_{\Gamma} V^{(\alpha)}(\xi) f_s(\xi)\,\mathrm{d}\xi \\ + \left(\tfrac{1}{3}K(b^3 - a^3), \tfrac{1}{3}(c^3 - a^3)\sin\sigma, \tfrac{1}{2}(b^2 - a^2)\right), \end{aligned} \tag{107}$$

after using (101) and (104) to expand $g(\xi, \sigma)$ and $g(\xi, \frac{1}{2}\pi)$. Remarkably we see that a combination of the functions $f_i(\xi)$, defined in (78) and (79), emerge from this process and hence we are able to write

$$\begin{aligned} \left(\frac{A_{ss} - M_t}{2\rho}, \frac{A_{rs}}{2\rho}, \frac{f_p}{-2K}\right) = \beta_0(d_0^{(\alpha)} + e_0^{(\alpha)}) + \boldsymbol{\beta}^{\mathrm{T}}(\mathbf{d}^{(\alpha)} + G\mathbf{e}^{(\alpha)}) \\ - \beta_0 \epsilon_0^{-1/2}(A_1^{(\alpha)} T_{11} + A_2^{(\alpha)} T_{21} + T_{1\alpha}) - \beta_0(A_1^{(\alpha)} T_{21} + A_2^{(\alpha)} T_{22} + T_{2\alpha}) \\ - (A_1^{(\alpha)} T_{s1} + A_2^{(\alpha)} T_{s2} + T_{s\alpha}) + \left(\tfrac{1}{3}K(b^3 - a^3), \tfrac{1}{3}(c^3 - a^3)\sin\sigma, \tfrac{1}{2}(b^2 - a^2)\right) \end{aligned} \tag{108}$$

where elements of $\mathbf{e}^{(\alpha)}$ are defined as $-e_n^{(\alpha)} \sinh p_n(\frac{1}{2}\pi - \sigma)/p_n$, $n \geq 1$. This step has involved a lot of algebra but the result is an expression which is straightforward to compute and simpler than using (21) directly.

The last part of the section is to calculate similar efficient expressions for the moments, $t_{s,r,p}$, defined by (23), or their proxies A_{sr}, A_{sr}. We are required to go through a similar procedure as above for the forces and thus only the final result of this calculation (see Crowley [4] for details). Thus

$$\left(\frac{A_{sr}}{2\rho}, \frac{A_{rr}}{2\rho}, \frac{t_p}{-2K}\right) = (\tau_0 - (\tfrac{1}{2}\pi - \sigma)e_0^{(r)})d_0^{(\alpha)} + \tau_0 e_0^{(\alpha)} + (\boldsymbol{\tau} + \mathbf{e}^{(r)})^{\mathrm{T}}\mathbf{d}^{(\alpha)} + \boldsymbol{\tau}^{\mathrm{T}}\mathsf{G}\mathbf{e}^{(\alpha)}$$
$$- \tau_0\epsilon_0^{-1/2}(A_1^{(\alpha)}\mathsf{T}_{11} + A_2^{(\alpha)}\mathsf{T}_{21} + \mathsf{T}_{\alpha 1})$$
$$- (\tau_0 - (\tfrac{1}{2}\pi - \sigma)e_0^{(r)})(A_1^{(\alpha)}\mathsf{T}_{12} + A_2^{(\alpha)}\mathsf{T}_{22} + \mathsf{T}_{\alpha 2}) - (A_1^{(\alpha)}\mathsf{T}_{1r} + A_2^{(\alpha)}\mathsf{T}_{2r} + \mathsf{T}_{\alpha r})$$
$$+ \left(\tfrac{1}{3}(c^3 - a^3)\sin\sigma, 0, \tfrac{1}{2}K^{-1}(b^2 - a^2)\right). \quad (109)$$

where

$$\boldsymbol{\tau} = -\mathbf{e}^{(r)} + (\tau_0 - (\tfrac{1}{2}\pi - \sigma)e_0^{(r)})\mathsf{P}\mathbf{C}_0 + \mathsf{P}\mathsf{G}\mathbf{e}^{(r)}, \quad (110)$$

and

$$\tau_0 - (\tfrac{1}{2}\pi - \sigma)e_0^{(r)} = -\frac{\mathbf{C}_0^{\mathrm{T}}\mathsf{P}\mathsf{G}\mathbf{e}^{(r)} + e_0^{(r)}}{\mathbf{C}_0^{\mathrm{T}}\mathsf{P}\mathbf{C}_0 + \mathsf{C}_{00}} \equiv -\frac{S_1^{(r)} + e_0^{(r)}}{S_2 + \mathsf{C}_{00}}, \quad (111)$$

in terms of previously-defined vectors and matrices.

The expression (109) is again straightforward to compute. It is possible, with some work, to confirm analytically from the expressions (91), (108) and (109) that the reciprocal relations (26) and (27) hold exactly.

5.5. Numerical approximation

All that remains is to develop numerical approximations to the matrix T in (82) in terms of solutions to (80). We follow methods outlined in, for example, Evans and Fernyhough [12], and expand the unknown functions $V_i(\xi)$ for $i = 1, 2, s, r, p$ in a finite series

$$V_i(t) \approx \sum_{r=0}^{R} \alpha_r^{(i)} v_r(t), \qquad \xi \in \Gamma \quad (112)$$

in terms of $R + 1$ unknown coefficients $\alpha_r^{(i)}$ and functions

$$v_r(t) = \frac{(-1)^r(2r)!\Gamma(\frac{1}{6})(\ln(b/c))^{1/6}}{2^{1/3}\pi\Gamma(2r + \frac{1}{3})}\left((\ln(b/c))^2 - (\ln b - t)^2\right)^{-1/3} C_{2r}^{1/6}\left(\frac{\ln b - t}{\ln(b/c)}\right), \quad (113)$$

expressed in terms of Gegenbauer polynomials, C_n^{ν}. This choice is made to incorporate the expected inverse cube root singularity in the velocity of the fluid at the corner of the wedge, or as $t \to \ln c$, whilst the wall condition (50) at $t = \ln b$ dictates that even Gegenbauer polynomials should be used. See, for example, Evans and Fernyhough [12]. The numerical pre-factor in (113)

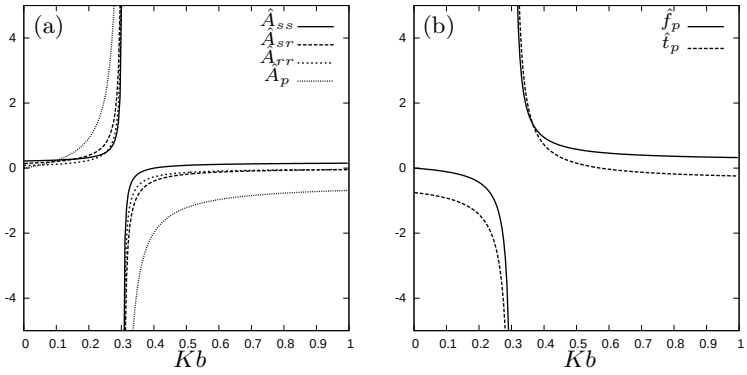

FIGURE 4: Variation of dimensionless hydrodynamic coefficients (in (a) $\hat{A}_{ss}$, $\hat{A}_{rs} = \hat{A}_{sr}$, $\hat{A}_{rr}$ and $\hat{A}_p$ and in (b) $-2\hat{q}_s = \hat{f}_p$ and $-2\hat{q}_r = \hat{t}_p$) against $Kb \equiv \omega^2 b/g$ for internal tank dimensions of $a/b = 0.5$, $c/b = 0.8$ such that the channel width ratio is 0.4, and $2\sigma = 0.8\pi$.

is chosen for subsequent algebraic simplification. Using (112) in the integral equation (80), multiplying through by $v_m(\xi)$, $m = 0, 1, \ldots, R$ and integrating over $\xi \in \Gamma$, a process which characterises the Galerkin method, gives rise to the following real, symmetric algebraic system of equations for the coefficients $\alpha_r^{(i)}$:

$$\sum_{r=0}^{R} \alpha_r^{(i)} K_{mr} = R_m^{(i)}, \qquad m = 0, 1, \ldots R \tag{114}$$

for each $i = 1, 2, s, r, p$ where

$$K_{mr} = \int_\Gamma \int_\Gamma K(t, \xi) v_m(\xi) v_r(t) \, \mathrm{d}\xi \, \mathrm{d}t, \qquad R_m^{(i)} = \int_\Gamma f_i(\xi) v_m(\xi) \, \mathrm{d}\xi. \tag{115}$$

Using the definition of K from (76) gives

$$K_{mr} = \sum_{n=1}^{\infty} \sum_{j=1}^{\infty} \frac{P_{nj} F_{mn}^I F_{rj}^I}{\cosh p_n(\frac{1}{2}\pi - \sigma) \cosh p_j(\frac{1}{2}\pi - \sigma)} + \sum_{n=1}^{\infty} \frac{F_{mn}^I F_{rn}^I}{p_n \coth p_n(\frac{1}{2}\pi - \sigma)} + \sum_{n=1}^{\infty} \frac{F_{mn}^{II} F_{rn}^{II}}{q_n \coth q_n \sigma} \tag{116}$$

where standard integral results (see Erdélyi et al. [8]) give, for $n \geq 1$

$$F_{mn}^I = \left(\frac{\ln(b/c)}{\ln(b/a)} \right)^{1/3} \frac{J_{2m+1/6}\left(\frac{\ln(b/c)}{\ln(b/a)} n\pi \right)}{(n\pi)^{1/6}} \qquad \text{and} \qquad F_{mn}^{II} = \frac{J_{2m+1/6}(n\pi)}{(n\pi)^{1/6}}. \tag{117}$$

Also, from the definitions of $f_i(\xi)$ in (78), (79) we find

$$R_m^{(1)} = \frac{\epsilon_0^{1/2}\delta_{m0}}{2^{2/3}\Gamma(\frac{7}{6})}\left(\frac{\ln(b/c)}{\ln(b/a)}\right)^{1/2} \tag{118}$$

in terms of the Kronecker delta symbol,

$$R_m^{(2)} = \sum_{n=1}^{\infty}\sum_{j=1}^{\infty}\frac{\mathsf{P}_{nj}\mathsf{C}_{j0}F_{mn}^I}{\cosh p_n(\frac{1}{2}\pi-\sigma)} \tag{119}$$

and

$$R_m^{(\alpha)} = \sum_{n=1}^{\infty}\sum_{j=1}^{\infty}\frac{\mathsf{P}_{nj}d_j^{(\alpha)}F_{mn}^I}{\cosh p_n(\frac{1}{2}\pi-\sigma)} + \sum_{n=1}^{\infty}\frac{e_n^{(\alpha)}F_{mn}^I}{p_n\coth p_n(\frac{1}{2}-\sigma)} + \sum_{n=1}^{\infty}\sum_{j=1}^{\infty}\frac{\mathsf{P}_{nj}e_j^{(\alpha)}F_{mn}^I}{\cosh p_n(\frac{1}{2}\pi-\sigma)\cosh p_j(\frac{1}{2}\pi-\sigma)} \tag{120}$$

for $\alpha = s, r, p$. Finally, the matrix elements are approximated by substituting (112) into (82) which results in

$$\mathsf{T}_{ij} \approx \sum_{r=0}^{R}\alpha_r^{(i)}R_m^{(j)}, \qquad i,j = 1,2,s,r,p. \tag{121}$$

Numerically it is found that values of T_{ij} computed using (114), (121) converge very rapidly with increasing truncation size R. This partly on account of the second-order accurate Galerkin method that has been employed but also because the choice of basis functions accurately reflects the fluid behaviour. In practice, R is taken to be of the order of 5 for 5 decimal place accuracy and so, numerically, the solution of (114) and the computation of (121) is very quick and accurate. Other infinite series occur in the process of making these calculations and therefore need truncation. It is found that the required 5 decimal places of accuracy is attained provided we truncate series over the index n to $N = 1000$ terms and series over the index j to 16 terms. The most numerically intensive part of this process is inverting matrix in the definition of P in (66).

A sample set of numerical results showing the variation of dimensionless added inertia coefficients, defined here as $\hat{A}_{ss} = A_{ss}/M_w$, $\hat{A}_{sr} = A_{sr}/(M_w b)$, $\hat{A}_{rr} = A_{rr}/(M_w b^2)$, $\hat{A}_p = A_p M_w\omega^2/b^2$, (where $M_w = \rho\pi b^2$ is the mass per unit length of fluid displaced by the submerged cylinder), moments, $\hat{t}_p = t_p/b^2$, and fluxes, $\hat{q}_r = q_r/b^2$, against dimensionless frequency Kb are shown in figures 4 and 5. Evident in these figures are values of Kb at which the various hydrodynamic coefficients asymptote towards plus/minus infinity. Unsurprisingly, these are identified as the natural undamped sloshing resonances of the internal tank whose resonant frequencies can be identified from figure 3. In the tank configuration with the smaller wedge section, the values of roll inertia and volume flux

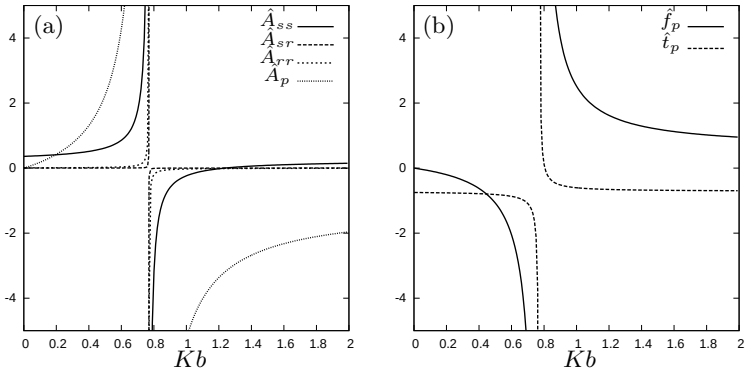

FIGURE 5: Variation of dimensionless hydrodynamic coefficients (in (a) $\hat{A}_{ss}$, $\hat{A}_{rs} = \hat{A}_{sr}$, $\hat{A}_{rr}$ and $\hat{A}_p$ and in (b) $-2\hat{q}_s = \hat{f}_p$ and $-2\hat{q}_r = \hat{t}_p$) against $Kb \equiv \omega^2 b/g$ for internal tank dimensions of $a/b = 0.5$, $c/b = 0.625$ such that the channel width ratio is 0.75, and $2\sigma = 0.2\pi$.

are seen to be smaller, as one would expect. It should also be noted that in the limit of $\omega \to 0$, $A_{ss} \to M_t$, the mass of the water in the tank.

The most severe test of the numerical method and the accuracy of the hydrodynamic coefficients is provided by the computation of the dimensionless version of Z_2, given by (37), namely $\hat{Z}_2 = Z_2 M_w \omega / b^2$, required in the evaluation of the wave power W. Thus, we confirm numerically that Z_2 remains bounded when the hydrodynamic coefficients diverge at the resonant frequency. This feature of the numerical results is rooted in the way in which have been able to express, in Section 5.4, the hydrodynamic coefficients in terms of elements of the T which preserves the reciprocal relations automatically and independently of the truncation parameters used in the numerical scheme. Similar boundedness in combinations of singular hydrodynamic coefficients has been reported in Evans and Newman [11] in a related problem and in Faltinsen and Timokha [13, §5.4.1.3]

6. Results

We focus now on the computation and optimisation of power from the fully coupled device. We shall consider only the case where the turbine power take-off parameter λ is real and constant. The dimensionless version of this will be reported, being $\hat{\lambda} = \lambda M_w \omega / b^2 \equiv \tilde{\lambda}\sqrt{Kb}$.

The success of the device relies on the power W being as high as possible over a broad range of wave frequencies typical of those found in a real sea spectrum (say 5-11s waves).

There are three components to W in the expression (44), each of which contributes to maximising the power. The first component is W_{max} itself and this

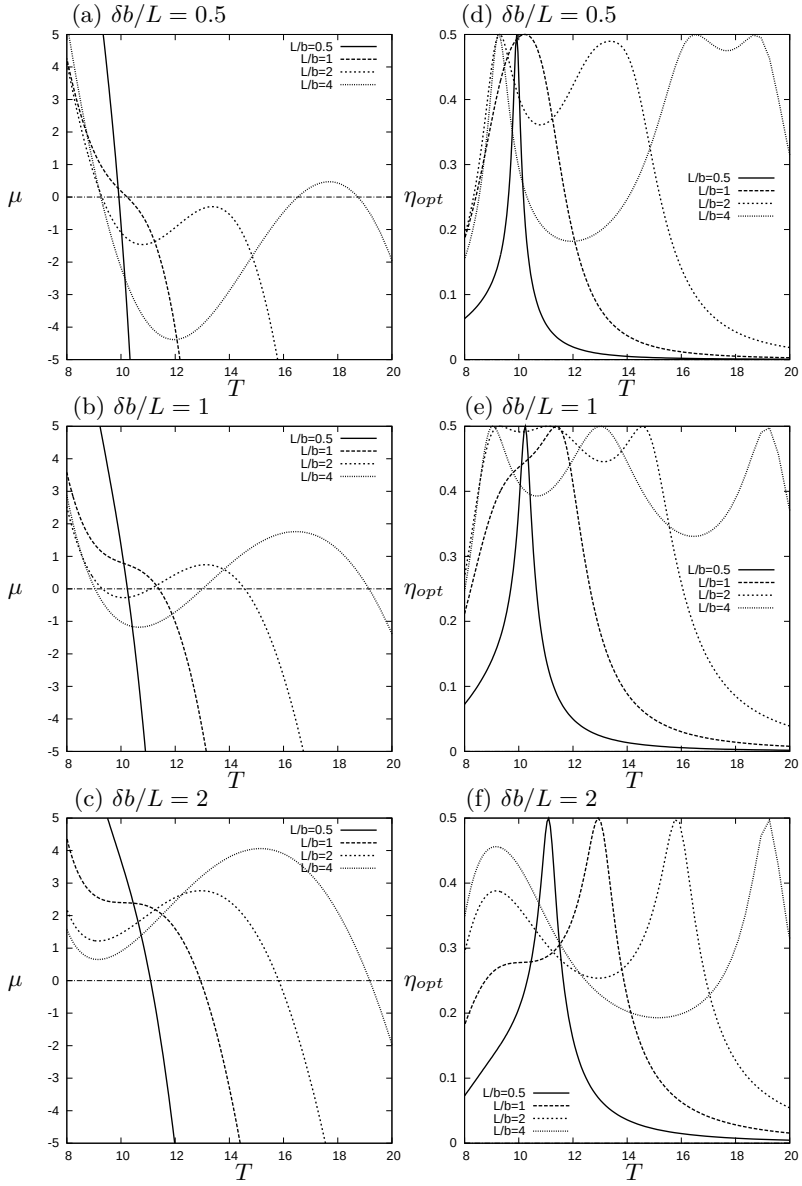

FIGURE 6: Values of μ and η_{opt} against period, T for a cylinder with $b = 7$m, $h = 50$m, $b/f = 0.75$, $M/M_w = 0.15$, and an internal tank with $a/b = 0.5$, $c/b = 0.8$, and $2\sigma = 0.8\pi$.

is a function of the geometry and motion of the WEC. This has elements which are fixed by the design of the device. That is, we are considering a submerged circular circular cylinder moving in surge motion. For a three-dimensional cylinder of finite length, the length, radius and submergence of the cylinder can all be adjusted to maximise W_{max} with respect to some measure of the size of the cylinder. Three-dimensional WECs of this type are normally assessed by their capture factor, being the ratio of W_{max} to the wave energy incident on the length of the WEC.

In two-dimensions, however, the situation is much more straightforward since all quantities are measured per unit length of the device and this naturally results in the efficiency, η, of the WEC, being the ratio of the power absorbed per unit length of the cylinder to the incident wave power per unit crest length. Thus, a symmetric device moving in surge the efficiency is well known (see, for example, Evans [9]) to be given by $\eta = W/(2W_{max})$ and takes a maximum of $\eta_{max} = \frac{1}{2}$, or 50% conversion efficiency. All computations below are based on this two-dimensional setting where efficiency is given by

$$\eta = \frac{1}{(1 + |Z_2|/\mathrm{Re}\{Z_2\})} \left(1 - \frac{(\lambda - |Z_2|)^2}{|\lambda + Z_2|^2}\right), \tag{122}$$

which has just two components to consider. The first, which represents the optimum efficiency for real λ, can be written

$$\eta_{opt} = \frac{1}{1 + \sqrt{1 + \mu}}, \qquad \text{where} \qquad \mu = \mathrm{Im}\{Z_2\}/\mathrm{Re}\{Z_2\} \tag{123}$$

and is thus dependent solely on the ratio μ. In particular, to maximise the efficiency (so that $\eta_{opt} = \eta_{max} = \frac{1}{2}$), this ratio needs to be zero. In practice we will aim to minimise μ over a broad range of wave frequencies – a task made easier if μ vanishes at multiple frequencies within the range of interest. Such zeros occur when $\mathrm{Im}\{Z_2\} = 0$ and these are identified as resonances of the coupled cylinder/tank configuration. The aim will be design the cylinder radius and submergence and the internal tank configuration to minimise μ. To maximise the second component, we must aim to choose a value of λ such that $\lambda \approx |Z_2|$ for the same broad range of frequencies. This is a tuneable condition but still, we will get the best results if $|Z_2|$ is approximately constant over the range of frequencies of interest.

We continue by presenting, in figures 6 and 7 two sets of results corresponding to the two internal tank configurations considered in figures 4 and 5 now coupled to a realistic mooring system in a physical setting. Thus, we have fixed the radius at $b = 7$m, the water depth to be 50m, the submergence of the cylinder at $b/f = 0.75$ equivalent to a clearance between the free surface and the top of the cylinder of 2.33m. Also fixed is the ratio of the mass of the cylinder to the mass of water displaced by the cylinder, $M/M_w = 0.15$. These parameters have been chosen as they are typical of those shown to perform well for a submerged cylinder WEC when internal mechanical systems of pendulums replace the internal water tank. In this dimensional setting we show the variation of the factor, μ, in the left-hand

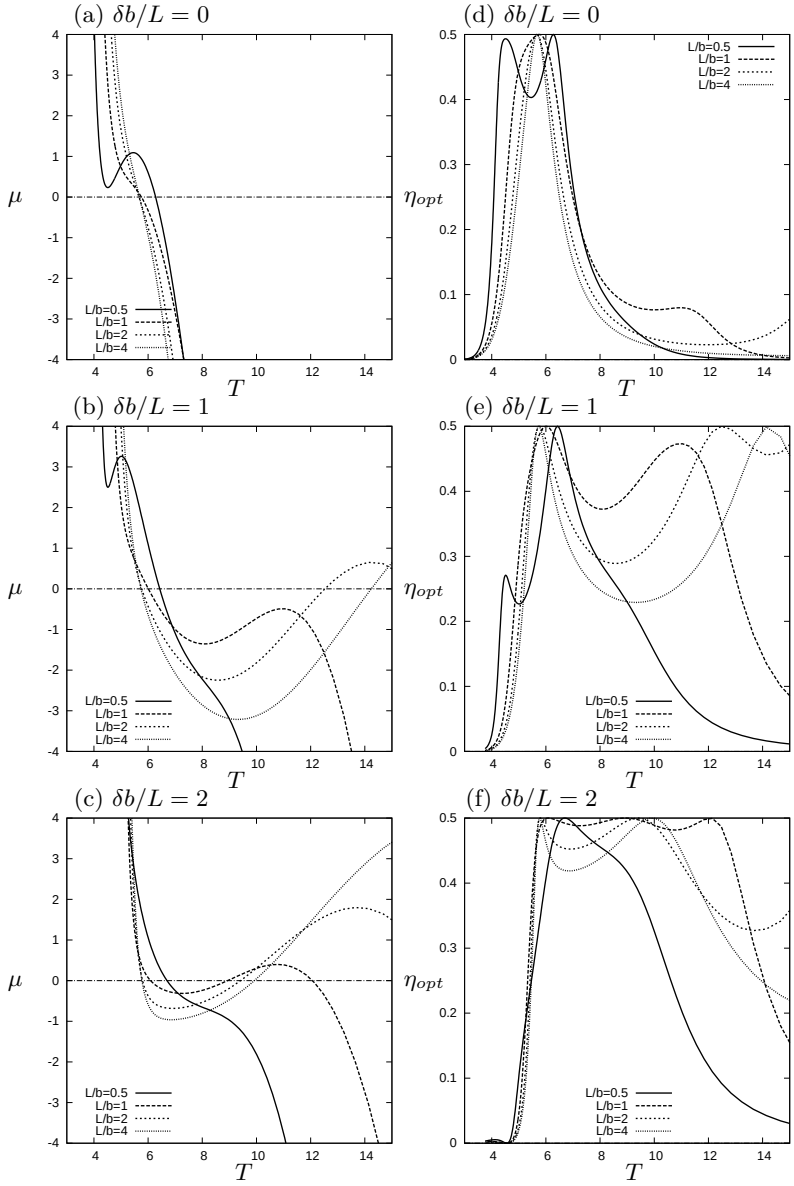

FIGURE 7: Values of μ and η_{opt} against period, T for a cylinder with $b = 7$m, $h = 50$m, $b/f = 0.75$, $M/M_w = 0.15$, and an internal tank with $a/b = 0.5$, $c/b = 0.625$, and $2\sigma = 0.2\pi$.

WEC	h (m)	b(m)	δ	b/f	L/b	s	c/b	a/c	$2\sigma/\pi$	$\tilde{\lambda}$	T
A	50	7	1	0.75	0.53	0.64	0.15	1.0	0.80	1.99	4.8
B	25	3.5	1	0.80	0.81	0.64	0.11	1.0	0.80	1.27	3.3
C	25	7	2	0.46	1.39	0.38	0.76	0.88	0.80	0.84	7.1

TABLE 1: Two-dimensional optimised configurations for a full scale and half scale device. Here s is the specific gravity given by $s = (M + M_t)/M_w$ and T is the natural sloshing period of the fluid in the tank.

figures and corresponding variations of optimal efficiency η_{opt} in the right-hand figures both against wave period, T. Apart from the tank configuration which is set as described in figures 4 and 5 the only degrees of freedom that are left to be defined are the length of the mooring system L, being the vertical distance between the midpoint of P_1 and P_2 or P shown in figure 1 and the centre O of the cylinder, and δ, which encapsulates the type of mooring system. On account of how the various terms are arranged within the equations, it turns out to make sense to plot curves of μ and η_{opt} against T for selected values of $\delta b/L$ and L/b; the values given to these parameters determine L and δ with $b = 7$m.

In figure 6 one clearly observes the correspondence between vanishing μ where the cylinder/tank are resonant and maximum $\eta_{opt} = \frac{1}{2}$. As also suggested if $|\mu|$ takes low values over a range of periods the η_{opt} will remain close to its maximum of $\frac{1}{2}$; the best example here is with $\delta b/L = 1$ and $L/b = 2$. It is not easy to understand mathematically how the multiple resonances, characterised by vanishing μ occur. Crowley et al. [3] show that the cylinder itself, without coupling to an internal resonant system can exhibit multiple resonances. In the example considered in figure 6 we note that the internal tank configuration is resonant at $T \approx 9.5$s and it is tempting to conclude from the figure shown that there is a signature of this internal resonance in each set of results shown.

However the system develops its response, the first point of note is that it is encouraging to find here that the sloshing of an internal fluid, driving air through the turbine, is capable of generating multiple resonances and hence multiple peaks in optimal efficiency across a broad range of periods.

In figure 7 a similar set of results are shown for a system with an internal tank configuration corresponding to the results shown in figure 5. Here, the sloshing resonance of the internal fluid is calculated to be at $T \approx 6$s and, again, results are suggestive of the influence of that resonance. The mooring configuration $\delta b/L = 2$ with $L/b = 1$ gives an impressive-looking broadbanded efficiency close to maximum over periods from $6 - 12$s.

The results provided by figures 6 and 7 serve as a guide as to the different types of results we might expect. It is evident that the mooring system $\delta = 0$, whilst capable of performing well over small range of periods, is not as broadbanded as for other values of δ.

By far the easiest mooring system to realise practically is that presented in

figure 1(b) for $\delta = 1$. For this reason we focus on the case $\delta = 1$ in addition to selected fixed values of either $b = 7$m, $h = 50$m (case A) or the half scale $b = 3.5$m, $h = 25$m (case B). However, we will now allow all other geometrical parameters including the mooring length, L, and submergence, f, as well as parameters, a, c and σ, associated with the internal tank configuration, to vary. Specifically these are to be considered as free variables within a numerical optimisation routine whose aim is to computationally determine the device parameters which maximise the power of the device over a range of wave periods. To avoid unphysical or impractical results constraints must be placed in the optimisation procedure on most of these variables. Of particular note we do not allow b/f to exceed 0.8 so that there is reasonable clearance between the top of the cylinder whilst the internal wedge angle 2σ cannot exceed 0.8π. The ratio M/M_w is fixed at 0.15. The objective function to be minimised in the optimisation routine is defined as the time-integral of $\frac{1}{2} - \eta$ over periods of 5s to 11s. This is not particularly sophisticated, but, by minimising this function, we are simply trying to achieve an evenly-weighted broadbanded efficiency across energetic wave periods belonging to a typical real sea state.

The results of this optimisation procedure are shown in table 1. This shows that, in both full scale and half scale examples A and B, the optimisation selects an annular tank with no internal wedge protrusion and a relatively small inner core. Indeed, the table show that the resonant wave periods for each of these two cases is well below the range of wave periods over which the optimisation is being performed. Contrary to the results suggested by figures 6 and 7 it appears that internal sloshing resonances are not essential for the successful performance of this WEC. Similar conclusions were drawn from the study of Crowley et al. [3] when the optimisation of the configuration of internal pendulums simiarly selected resonant periods below the target period range. The particular conclusion drawn in that paper might apply here also; that it is the pitching cylinder resonance itself which is the principal component in making this device work. The internal water tank acts instead as an inertial device against which relative rotation of the cylinder under motion produces power.

In the final line of table 1 we consider a further set of fixed values of $b = 7$m and $h = 25$m with $\delta = 2$ (case C) and with an added constraint that the mooring is attached to the sea bed. Here, the optimiser selects a tank configuration which *does* include an internal wedge whose resonance period of $T = 7.1$s appears important.

In figure 8 we show how the two optimised cases A and B operate. Figure 8(a) demonstrates that a high broadbanded maximum efficiency is possible for the full size cylinder (case A), associated with μ being close to zero over a wide range of frequencies and $|\hat{Z}_2|/\sqrt{Kb}$ not varying far from the optimal value of $\tilde{\lambda}$ selected by the optimiser. Figure 8(d) shows the associated maximum pitch angle of the cylinder per unit wave amplitude (that is, per 2m wave height) which can readily be computed from the solution. Case A looks fairly reasonable, confined to about 16° though case B is far in excess of the limits under which linearised theory should be used. Clearly, for larger wave heights the theory presented here is not applicable. The results of case B suggest that the cylinder

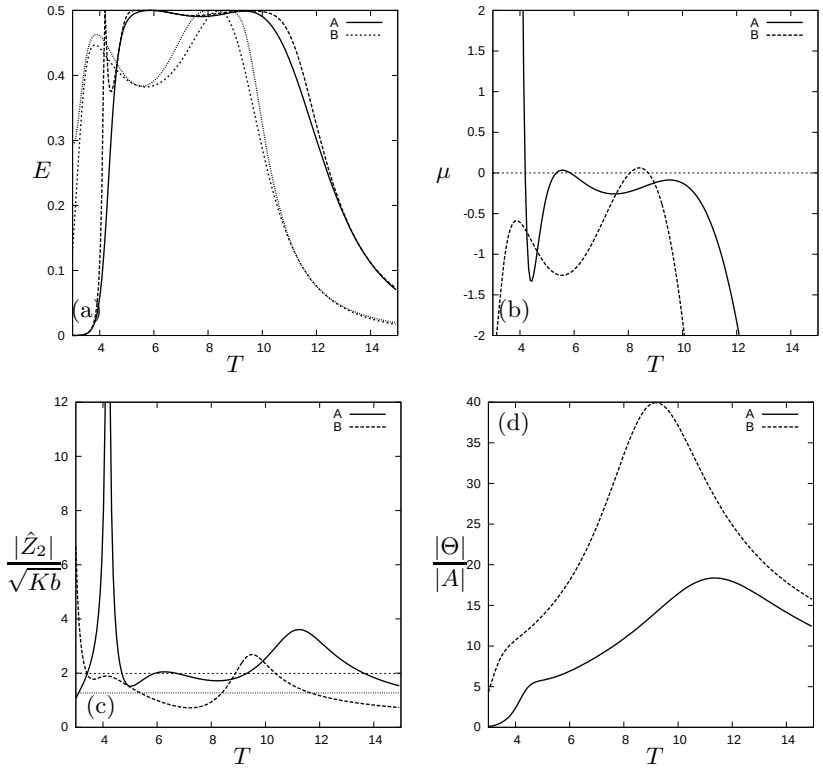

FIGURE 8: Results for the optimised pitching cylinder devices A & B detailed in table 1: (a) the efficiency E bounded above by its optimal value E_{opt}; (b) μ; (c) $|\hat{Z}_2|/\sqrt{Kb}$; (d) the maximum angular excursion $|\Theta/A|$ per unit wave amplitude in degrees.

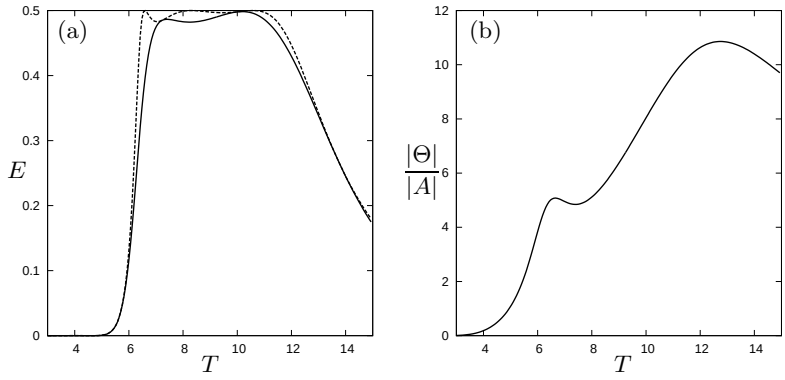

FIGURE 9: Results for the optimised pitching cylinder device C detailed in table 1: (a) the efficiency E and its optimal value E_{opt} and (b) the excursion of the device $|\Theta/A|$.

here is too small to convert high proportions of incident wave energy and, when tuned to do so, is forced into large pitching excursions.

We return briefly to case C and show its efficiency curve and cylinder excursion in figure 9. Here, with the bigger cylinder, a high broadbanded efficiency is returned and, with the $\delta = 2$ mooring attached to the sea bed inducing twice the cylinder roll angle than in cases A and B the cylinder pitch excursions are reduced from those seen for $\delta = 1$ in figure 8.

7. Conclusions

We have presented a preliminary investigation into the operation of a submerged cylinder wave energy converter with an internal power take off system based on sloshing fluid motion. It has been demonstrated that the motion of a pitching cylinder close to the free surface coupled to the pitch-induced roll of the cylinder itself driving the internal water motion can create multiple resonances and resulting broadbanded power take off characteristics. Towards the end we have focussed on one particular embodiment for the size location and mooring of the cylinder and used numerical optimisation to identify the best configuration under these conditions. The flexibility offered by different mooring systems has not been fully explored here. Nor have we considered other practical constraints that might need to be imposed on the system such as limiting the amplitude of the motion or increasing the submergence of the cylinder. With the number and flexibility of the parameters available it may be possible to consider other solutions and retain a high broadbanded efficiency.

During the paper we have shown how to determine sloshing frequencies and forced motion hydrodynamic coefficients for fluid in a tank with a novel and complex geometrical configuration. This has been done using powerful mathematical techniques resulting in accurate and efficient numerical results.

Appendix A: The centre of gravity of the cylinder

Here we make the calculation of the centre of gravity of the tank in figure 2(a),

$$z_G + f = -\frac{\rho_c}{M} \int_{\delta V} \boldsymbol{r}_z \, \mathrm{d}V = \tfrac{2}{3}(c^3 - a^3) \sin\sigma \frac{\rho_c}{M}, \tag{124}$$

where ρ_c is the density of the internal mass of the solid cylinder and M the mass of the cylinder without the internal fluid. The z-component of the position vector $\boldsymbol{r} = (r\sin\theta, r\cos\theta)$ with respect to the centre of the cylinder is integrated over the internal region of the cylinder, where only the wedge section $a < r < c$, $-\sigma < \theta < \sigma$ makes a net contribution away from $z_G = -f$. The turbine is neglected in this calculation.

References

[1] A. Babarit, A.H. Clement, J. Ruer, C. Tartivel, SEAREV: A fully integrated wave energy converter, Proc. OWEMES, (2006).

[2] A. Babarit, J. Hals, A. Muliawan, T. Moan, J. Krokstad, Numerical benchmarking study of a selection of wave energy converters, Renewable Energy 41, (2012) 44–63.

[3] S.H. Crowley, R. Porter, D.V. Evans, A submerged cylinder wave energy converter, Journal of Fluid Mechanics 716, (2013) 566–596.

[4] S.H. Crowley, Absorbing energy using coupled resonances, Ph.D. Thesis, University of Bristol (2013).

[5] R. Clare, D.V. Evans, T.L. Shaw, Harnessing sea wave energy by a submerged cylinder device, ICE Proceedings 73(3), (1982) 565–585.

[6] J. Cruz, Ocean wave energy: current status and future perspectives. Springer: Green Energy and Technology (2008).

[7] J. Cruz, S.H. Salter, Numerical and experimental modelling of a modified version of the Edinburgh Duck wave energy device. Proceedings of the IMechE. Part M: Engineering for the Maritime Environment 220(3), (2006) 129–147.

[8] A. Erdélyi, W. Magnus, F. Oberhettinger, F.G. Tricomi, Tables of Integral Transforms, McGraw-Hill (1954).

[9] D.V. Evans, A theory for wave-power absorption by oscillating bodies, Journal of Fluid Mechanics 77, (1976) 1–25.

[10] D.V. Evans, R. Porter, Wave energy extraction by coupled resonant absorbers, Philosophical Transactions of the Royal Society of London A. 370(1959), (2012) 315–344.

[11] D.V. Evans, J.N. Newman, A wave energy converter with an internal water tank, Proceedings of the 26th International Workshop on Water Wave and Floating Bodies, Athens, Greece (2011).

[12] D.V. Evans, M. Fernyhough, Edge waves along periodic coastlines. Part 2, Journal of Fluid Mechanics, 297, (1995) 307–326,

[13] O.M. Faltinsen, A.N. Timokha, Sloshing. Cambridge University Press (2009).

[14] D.W. Fox, J.R. Kuttler, Sloshing frequencies, Zeitschrift für Angewandte Mathematik und Physik (ZAMP), 34(5), (1983) 668–696.

[15] S.H. Salter, Wave power, Nature 249, 5459 (1974), 720–724.

[16] A. Sarmento, A.F.O. Falcão, Wave generation by an oscillating surface-pressure and its application in wave-energy extraction, Journal of Fluid Mechanics 150, (1985) 467–485.

[17] T.J.T Whittaker, M. Folley, Nearshore oscillating wave surge converters and the development of Oyster, Philosophical Transactions of the Royal Society of London A. 370(1959), (2012) 345–364.